

1 Characterization of the Photophysical, Thermodynamic, and 2 Structural Properties of the Terbium(III)–DREAM Complex

3 Walter G. Gonzalez,[†] Victoria Ramos,[†] Maurizio Diaz,[‡] Alyssa Garabedian,[†] Camilo Molano,[†]
4 Francisco Fernandez-Lima,^{†,§} and Jaroslava Miksovská^{*,†,‡,§}

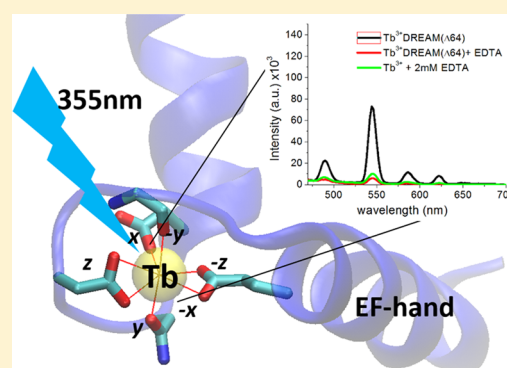
5 [†]Department of Chemistry and Biochemistry, Florida International University, Miami, Florida 33199, United States

6 [‡]School for Advanced Studies Homestead, Homestead, Florida 33030, United States

7 [§]Biomolecular Science Institute, Florida International University, Miami, Florida 33199, United States

8 **S** Supporting Information

9 **ABSTRACT:** DREAM (also known as K⁺ channel interacting protein 3 and
10 calsenilin) is a calcium binding protein and an active modulator of K_v4
11 channels in neuronal cells as well as a novel Ca²⁺-regulated transcriptional
12 modulator. DREAM has also been associated with the regulation of
13 Alzheimer's disease through the prevention of presenilin-2 fragmentation.
14 Many interactions of DREAM with its binding partners (Kv4, calmodulin,
15 DNA, and drugs) have been shown to be dependent on calcium. Therefore,
16 understanding the structural changes induced by binding of metal to
17 DREAM is essential for elucidating the mechanism of signal transduction
18 and biological activity of this protein. Here, we show that the fluorescence
19 emission and excitation spectra of the calcium luminescent analogue, Tb³⁺,
20 are enhanced upon binding to the EF-hands of DREAM due to a mechanism
21 of energy transfer between Trp and Tb³⁺. We also observe that unlike Tb³⁺-
22 bound calmodulin, the luminescence lifetime of terbium bound to DREAM
23 decays as a complex multiexponential ($\tau_{\text{average}} \sim 1.8$ ms) that is sensitive to perturbation of the protein structure and drug
24 (NS5806) binding. Using isothermal calorimetry, we have determined that Tb³⁺ binds to at least three sites with high affinity (K_d
25 = 1.8 μM in the presence of Ca²⁺) and displaces bound Ca²⁺ through an entropically driven mechanism ($\Delta H \sim 12$ kcal mol⁻¹,
26 and $T\Delta S \sim 22$ kcal mol⁻¹). Furthermore, the hydrophobic probe 1,8-ANS shows that Tb³⁺, like Ca²⁺, triggers the exposure of a
27 hydrophobic surface on DREAM, which modulates ligand binding. Analogous to Ca²⁺ binding, Tb³⁺ binding also induces the
28 dimerization of DREAM. Secondary structural analyses using far-UV circular dichroism and trapped ion mobility spectrometry–
29 mass spectrometry reveal that replacement of Ca²⁺ with Tb³⁺ preserves the folding state with minimal changes to the overall
30 structure of DREAM. These findings pave the way for further investigation of the metal binding properties of DREAM using
31 lanthanides as well as the study of DREAM–protein complexes by lanthanide resonance energy transfer or nuclear magnetic
32 resonance.



33 DREAM (downstream regulatory element antagonist modu-
34 lator), also named KChIP3 and calsenilin, is a 29 kDa
35 multifunctional Ca²⁺-sensing protein found in different neuro-
36 nal cell compartments.¹ Outside the nucleus, DREAM interacts
37 with presenilin to regulate amyloid precursor protein
38 processing and with potassium channels to regulate their
39 membrane translocation and gating.^{2,3} Moreover, DREAM
40 represents a new class of Ca²⁺-sensing protein that can
41 translocate to the nucleus and directly bind DNA.¹ In the
42 nucleus, it regulates prodynorphin and c-fos gene expression by
43 binding to the DRE regulatory sequence of those genes.^{1,4}
44 Association of DREAM with the DRE promoter regions in the
45 absence of calcium leads to inhibition of gene transcription.
46 These genes have been shown to be involved in apoptosis, cell
47 homeostasis, and pain modulation.^{5,6} The role of DREAM in
48 pain sensing, memory retention, learning, and Alzheimer's
49 disease highlights the multifunctional properties of this
50 protein.⁶ As a calcium signal transducer, DREAM does not

possess endogenous catalytic activity, and its regulatory effect in
51 biological processes arises from interaction with numerous
52 binding partners. Therefore, understanding how calcium and
53 other metals trigger structural changes in DREAM, and how
54 this protein reorganization controls target recognition, would
55 provide important insight into its mechanism of action.
56

The three-dimensional structure of Ca²⁺-bound DREAM has
57 been obtained through nuclear magnetic resonance (NMR)
58 and is presented in Figure 1a.⁷ DREAM has four EF-hand
59 motifs; EF-hand 3 and EF-hand 4 are able to bind Ca²⁺, while
60 EF-hand 1 is unable to bind either Mg²⁺ or Ca²⁺. The
61 coordination of calcium/magnesium in the EF-hand motif has
62 been widely studied, and it has been shown to form hexa- or
63 heptacoordination with oxygen atoms of proteins to form a 64

Received: January 27, 2016

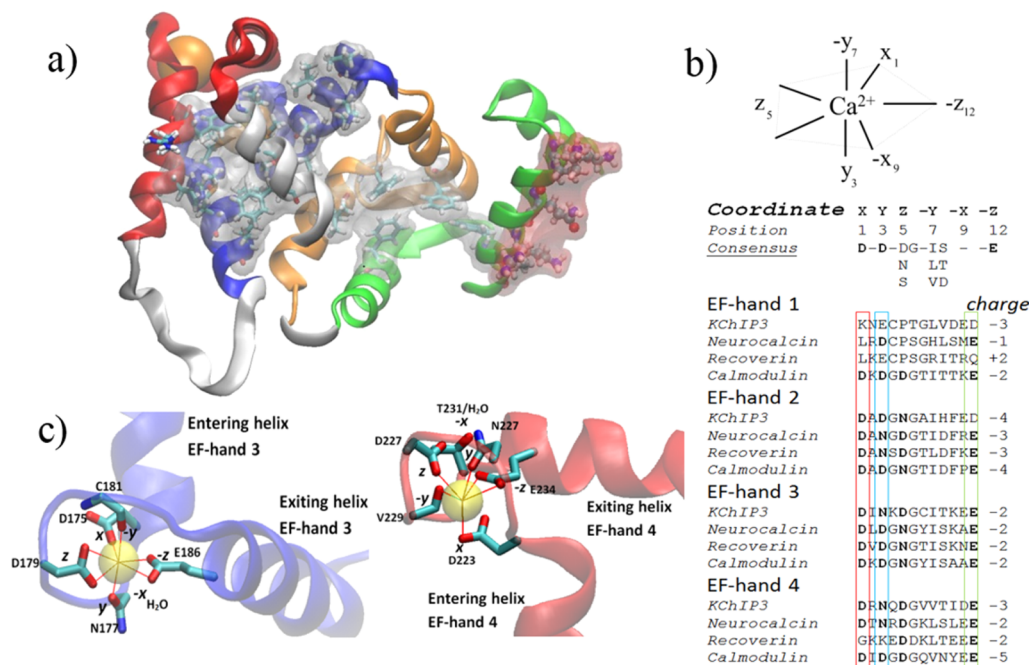


Figure 1. (a) NMR structure of DREAM monomer with highlighted hydrophobic residues (gray mesh) and charged residues (red mesh) (Protein Data Bank entry 2JUL).⁷ The four EF-hands of DREAM are colored green (EF-hand 1), orange (EF-hand 2), blue (EF-hand 3), and red (EF-hand 4). Calcium is shown as an orange sphere. (b) Coordination geometry of calcium bound to EF-hand 3 (left) and EF-hand 4 (right). Residues involved in coordination of Ca^{2+} are shown as a licorice model. EF-hand 3 shows a clear pentagonal bipyramidal coordination, whereas EF-hand 4 is distorted. (c) Geometry and consensus sequence of EF-hand binding loops as well as sequence homology between neuronal calcium sensors and calmodulin at the metal binding loops.

65 pentagonal bipyramidal coordination (Figure 1b,c).^{8,9} The
 66 oxygen-donating amino acids of the calcium selective metal
 67 binding loop in EF-hands follow a common organization such
 68 that positions 1, 3, and 5 are either an aspartic or an asparagine
 69 amino acid while the amino acid at position 12 is a well-
 70 conserved glutamic acid (Figure 1b). Modulation of metal
 71 affinity and selectivity arises from distinct combinations of
 72 negatively charged amino acids at these positions. For instance,
 73 EF-hand 2 of DREAM has been proposed to selectively bind
 74 Mg^{2+} due to Glu \rightarrow Asp mutation at position 12, which
 75 eliminates the heptacoordination necessary for strong binding
 76 of Ca^{2+} .^{10,11} Similarly, the presence of a lysine at position 1,
 77 proline at position 5, and aspartic acid at position 12 renders
 78 EF-hand 1 of DREAM unable to bind most metals.^{10,12}

79 Association of calcium at the metal binding loop of the active
 80 EF-hand pair at the C-terminus of DREAM induces a structural
 81 rearrangement that leads to exposure of a hydrophobic surface
 82 as well as changes in oligomerization state.^{12,13} However, details
 83 about the underlying molecular mechanism by which calcium
 84 binds and induces structural changes in DREAM are not
 85 known. Nonetheless, experiments using NMR to monitor the
 86 glycine residues in the EF-hand loops and the associated
 87 chemical shift broadening upon metal binding would provide
 88 insight into the role of amino acids of DREAM. Of particular
 89 interest is the use of lanthanide ions, which have been shown to
 90 possess physical properties similar to those of calcium ions and
 91 have been widely applied to study the metal binding properties
 92 of EF-hands.^{14,15} Additionally, lanthanide–protein complexes
 93 have been shown to undergo magnetic alignment during NMR
 94 experiments, which is of great help in elucidating the three-
 95 dimensional structure of protein–metal and protein–protein
 96 complexes.¹⁷ The advantage of employing lanthanides to

understand the mechanism of calcium binding is their unique
 97 luminescence properties as well as their ability to effectively
 98 displace calcium from EF-hand loops. Replacement of Ca^{2+}
 99 with Tb^{3+} has also been shown to induce structural changes in
 100 the EF-hand loops that are highly homologous to those
 101 observed upon calcium binding.¹⁶ In this report, we implement
 102 a combination of fluorescence, luminescence, TIMS–MS, and
 103 calorimetric techniques to show that Tb^{3+} binds at the EF-
 104 hands of DREAM and functions as a calcium biomimetic.
 105 Moreover, we show that association of Tb^{3+} at EF-hands 3 and
 106 4 of DREAM leads to a calcium-like conformation with
 107 hydrophobic surface exposure, oligomeric transition, and ion-
 108 neutral collisional cross section (CCS) similar to those
 109 observed for the Ca^{2+} -bound protein. Nonetheless, we observe
 110 small deviations in the dynamics of the environment near
 111 Trp169 as well as secondary structure organization, indicating
 112 that not all aspects of Tb^{3+} binding are identical to those of
 113 Ca^{2+} binding. Using ITC and the fluorescence properties of
 114 Tb^{3+} , we are able to gain insight into the role of Mg^{2+} and
 115 ligand binding to DREAM. Initial results of this study have
 116 been previously presented in an abstract form.¹⁸ 117

118 ■ MATERIALS AND METHODS

General. NS5806 {1-[2,4-dibromo-6-(1H-tetrazol-5-yl)-
 119 phenyl]-3-(3,5-bis-trifluoromethyl-phenyl)urea, >99% pure}
 120 was purchased from Tocris Bioscience, trifluoperazine (TFP)
 121 from Sigma-Aldrich, and 1,8-ANS (8-anilino-1-naphthalenesul-
 122 fonic acid) from Cayman Chemical Co. Concentrated stock
 123 solutions were prepared as previously described.¹⁹ $\text{TbCl}_3 \cdot 6\text{H}_2\text{O}$
 124 was obtained from Sigma-Aldrich and used without further
 125 purification. Terbium stocks of ~ 0.5 M were prepared
 126 gravimetrically in decafiltered ultrapure 18 M Ω water, and the
 127

128 concentrations of Tb³⁺ stocks were confirmed by titrations
129 against EDTA standards.

130 Isolation and Purification of DREAM Constructs.

131 Recombinant mouse DREAM(Δ 64), DREAM(Δ 160), and
132 DREAM(Y174A) constructs were expressed in *Escherichia coli*
133 BL21(DE3) cells and purified according to previously
134 published procedures.^{12,20} Two additional protein constructs
135 with single-amino acid mutations of glutamic acid at position 12
136 in the loop of EF-hand 3 and EF-hand 4 were obtained and are
137 named DREAM(E186Q) and DREAM(E234Q), respectively.
138 Rat calmodulin was purified as previously described.^{19,21}

139 **Photophysics of the DREAM:Tb³⁺ Complex.** Fluores-
140 cence experiments were conducted on a custom PC1-
141 ChronosFD instrument (ISS, Champaign, IL) in steady-state
142 mode for excitation and emission spectra and in frequency
143 domain mode for fluorescence decay measurements. The
144 intrinsic protein fluorescence arising from tyrosine residues in
145 CaM and tryptophan on DREAM was obtained by exciting the
146 sample with 280 \pm 2 and 295 \pm 2 nm light, respectively. The
147 fluorescence of 1,8-ANS was monitored by exciting the sample
148 with 350 \pm 4 nm light, through a vertically oriented polarizer.
149 The sensitized emission spectra of terbium(III)-bound proteins
150 were obtained by exciting the sample at 280 \pm 4 nm while
151 collecting the emission through a 400 nm long pass filter to
152 minimize the contribution of the protein intrinsic fluorescence
153 and the second harmonic peaks. Displacement of Ca²⁺ from
154 DREAM was monitored by adding small aliquots of a 2.0 mM
155 Tb³⁺ in 20 mM TRIS (pH 7.4) stock solution to 10–20 μ M
156 DREAM construct in the same buffer with 5 mM Mg²⁺ and/or
157 100 μ M Ca²⁺. The resulting spectra were normalized by
158 dividing the intensity at each wavelength by the background
159 value at 530 nm, and the resulting titration plots were fitted
160 using a noncooperative n-site quadratic equation that assumes a
161 similar affinity for all the sites.²⁰ All spectra were corrected for
162 the PMT wavelength-dependent response as well as the lamp
163 wavelength-dependent changes in intensity. The intrinsic
164 fluorescence lifetime of DREAM was measured by exciting
165 the sample with the modulated light of a 280 nm diode, and the
166 fluorescence collected through a 320 nm long pass filter with
167 2,5-diphenyloxazole (PPO) in ethanol (τ = 1.40 ns) used a
168 lifetime reference.

169 Circular dichroism measurements were conducted in a Jasco
170 J-815 CD spectrometer along the 1 mm path of a quartz cuvette
171 (model J-815, Jasco, Easton, MD). Luminescence measure-
172 ments were conducted on a home-built instrument where the
173 sample was placed in a 2 mm \times 10 mm quartz cuvette in a
174 temperature-controlled sample holder (Quantum Northwest,
175 Liberty Lake, WA) and excited along the 10 mm path. The 355
176 nm line of a Nd:YAG laser (Minilite II Continuum, San Jose,
177 CA) was used to directly excite Tb³⁺ ions, while the
178 luminescence was measured perpendicularly through a 550 \pm
179 10 nm band-pass filter and detected by a H7360-01 PMT
180 (Hamamatsu). The signal was digitized by a 400 MHz
181 oscilloscope (WaveSurfer 42Xs, Teledyne Lecroy), and the
182 initial 100 μ s of each trace was deleted to eliminate the
183 contribution from scattered light and PMT recovery time. The
184 fluorescence modulation-phase plots and luminescence decay
185 traces were fit using Globals for spectroscopy software (LFD,
186 Irvine, CA).

187 Thermodynamics of the DREAM:Tb³⁺ Complex.

188 Isothermal calorimetry titrations were employed to determine
189 the thermodynamics of Tb³⁺ displacement of Ca²⁺ from
190 DREAM or CaM and were conducted using a VP-ITC

isothermal calorimeter (Microcal Inc., Northampton, MA).
191 Protein constructs were dialyzed overnight in 5 mM TRIS (pH
192 7.4), 100 mM NaCl, and 100 μ M CaCl₂ with or without 5 mM
193 MgCl₂. The use of 10 mM EDTA during purification of
194 calmodulin required multiple overnight dialysis steps to ensure
195 complete removal of contaminating EDTA. Terbium stock
196 solutions were prepared in ITC dialysate buffer. The reaction
197 cell was loaded with an \sim 10 μ M protein solution, determined
198 spectrophotometrically prior to the ITC experiment, and the
199 concentration of Tb³⁺ in the syringe (297 μ L) was 1.00 mM.
200 Thirty injections of increasing volume were titrated into the
201 protein solution with increasing time intervals between
202 injections. Isotherms were corrected for the heat of dilution
203 of ligand, and all ITC experiments were conducted in triplicate.
204 The recovered thermodynamic parameters were obtained by
205 fitting the isotherms modeled either with an *N*-set-of-sites
206 model or with a sequential model using the Microcal ITC
207 analysis plug in Origin 7.0. 208

209 **Trapped Ion Mobility Spectrometry–Mass Spectrom-**
210 **etry (TIMS–MS) Studies.** *Experimental Section.* Details
211 regarding the TIMS operation and specifics compared to
212 traditional IMS can be found elsewhere.^{22–25} Briefly, in TIMS,
213 mobility separation is based on holding the ions stationary
214 using an electric field against a moving gas. The separation in a
215 TIMS device can be described by the center of the mass frame
216 using the same principles as in a conventional IMS drift tube.²⁶
217 The TIMS analyzer was coupled to a maXis Impact Q-UHR-
218 ToF instrument (Bruker Daltonics Inc., Billerica, MA). Data
219 acquisition was controlled using in-house software, written in
220 National Instruments Lab VIEW (2012, version 12.0f3) and
221 synchronized with the maXis Impact acquisition program.
222 TIMS separation was performed using nitrogen as a bath gas at
223 \sim 300 K, and typical *P*₁ and *P*₂ values are 1.8 and 0.6 mbar,
224 respectively. The same RF (880 kHz and 200–350 Vpp) was
225 applied to all electrodes, including the entrance funnel, the
226 mobility separating section, and the exit funnel. Protein samples
227 were prepared at 15 μ M protein and 15 μ M TbCl₃·6H₂O using
228 HPLC grade solvents from Thermo Fisher Scientific Inc.
229 (Waltham, MA) in 10 mM ammonium acetate under
230 physiological conditions (pH 6.7). A custom-built, nano-
231 electrospray ionization source was coupled to the TIMS–MS
232 analyzer and was used for all analyses. A typical source voltage
233 of 600–1200 V was used, and analyses were performed in
234 positive ion mode.

235 *Theoretical.* Theoretical CCS were calculated for the
236 previously reported 2JUL NMR structure of DREAM⁷ using
237 IMoS (version 1.04b)^{27–29} with nitrogen as a bath gas at \sim 300
238 K. In the IMoS calculations, 100 total rotations were performed
239 using the diffuse hard sphere scattering method with a Maxwell
240 distribution. 240

241 ■ RESULTS

242 The well-known calcium biomimetic behavior of europium-
243 (III), terbium(III), and neodymium(III) and the unique
244 spectroscopic properties of protein:lanthanide complexes have
245 been widely employed to characterize the sequence of metal
246 binding to calcium binding proteins,^{30–32} to observe protein
247 conformational heterogeneity,³³ to determine water coordina-
248 tion of metals bound at the EF-hand motif,³⁴ and as binding
249 assays.³⁵ Therefore, we envisioned that the properties of
250 lanthanides could be employed to obtain information about the
251 biophysical properties of DREAM protein. However, the
252 association of lanthanides with the KChIP subfamily of calcium

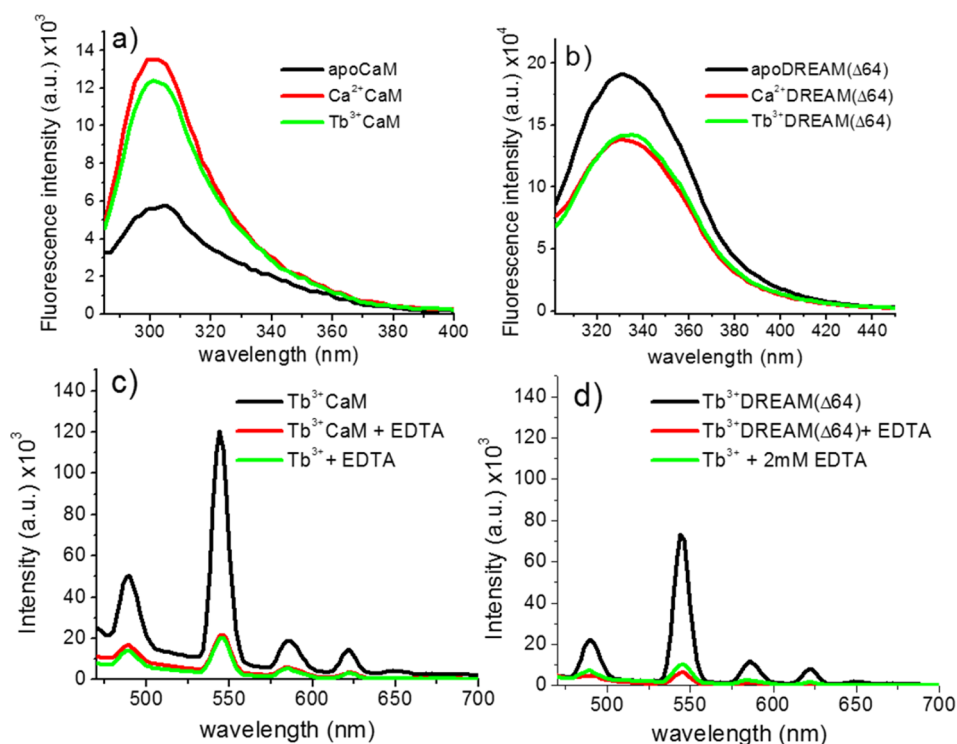


Figure 2. Intrinsic fluorescence changes of 40 μM (a) CaM and (b) DREAM($\Delta 64$) upon binding of 1 mM calcium or 160 μM Tb^{3+} on CaM or 80 μM Tb^{3+} for DREAM($\Delta 64$), excited at 280 ± 4 nm. The observed tyrosine fluorescence change upon binding of Tb^{3+} to CaM shows a small deviation from that observed for Ca^{2+} , likely due to quenching of the fluorescence by energy transfer to Tb^{3+} . The Tb^{3+} -induced transition for DREAM($\Delta 64$) is identical to that observed in the presence of Ca^{2+} . Sensitized emission of (c) 160 μM Tb^{3+} bound to CaM and (d) 80 μM Tb^{3+} bound to DREAM($\Delta 64$), excited at 280 nm with and without 2 mM EDTA. The background emission of the Tb^{3+} :EDTA complex is shown as a reference. The observed sensitized emission of Tb^{3+} shows the characteristic sharp bands at 489, 544 (major), 586, and 622 nm due to the $^5\text{D}_4 \rightarrow ^7\text{F}_6$, $^5\text{D}_4 \rightarrow ^7\text{F}_5$, $^5\text{D}_4 \rightarrow ^7\text{F}_4$, and $^5\text{D}_4 \rightarrow ^7\text{F}_3$ transitions of Tb^{3+} , respectively. The major peak at 545 nm for DREAM($\Delta 64$) is 40% smaller than that observed for CaM. Addition of 2 mM EDTA to either CaM or DREAM($\Delta 64$) resulted in an emission identical to that of Tb^{3+} in solution.

253 binding proteins has not been extensively studied. Thus, we
 254 first set forth to determine whether Tb^{3+} can directly associate
 255 with the EF-hand of DREAM. This is important, because
 256 previous studies of DREAM($\Delta 64$) using mass spectrometry
 257 and studies of NCS-1 using sensitized emission have presented
 258 contradicting results on whether Tb^{3+} can bind to neuronal
 259 calcium sensors.^{10,36} Additionally, we are interested in
 260 investigating whether Tb^{3+} binding induces structural changes
 261 in DREAM homologous similar to those observed for calcium.

262 **Terbium(III) Binds to DREAM and Is Sensitized by**
 263 **Energy Transfer from W169.** Calmodulin and DREAM are
 264 well-known to undergo distinct structural changes upon
 265 binding of calcium, which are accompanied by changes in
 266 fluorescence of tyrosine and tryptophan residues, respec-
 267 tively.^{1,37} These fluorescence transitions are shown in panels
 268 a and b of Figure 2. When calcium binds, the tyrosine
 269 fluorescence of CaM increases whereas the tryptophan
 270 fluorescence of DREAM decreases, in agreement with previous
 271 reports. Of particular interest is the observation that in the
 272 presence of Tb^{3+} , at molar ratios of 4:1 for CaM and 2:1 for
 273 DREAM, the fluorescence emission is nearly identical to that
 274 observed in the presence of saturating calcium (Figure 2a,b).
 275 The slightly lower tyrosine fluorescence of CaM in the presence
 276 of Tb^{3+} is likely due to an efficient quenching of Tb^{3+} by an
 277 aromatic amino acid or due to incomplete binding of this ion.
 278 We also investigated whether binding of Tb^{3+} on DREAM leads
 279 to the transfer of energy from nearby aromatic residues toward
 280 the metal ligand, as previously observed for CaM.³² The
 281 presence of the characteristic sharp emission bands in the

282 sensitized emission spectra of the DREAM($\Delta 64$): Tb^{3+} complex
 283 supports the idea that aromatic residues, likely at the C-
 284 terminus of DREAM, are able to transfer energy to bound
 285 terbium (Figure 2c,d). The sensitized emission intensity of
 286 terbium bound to DREAM($\Delta 64$) is approximately half of that
 287 observed for CaM, which is likely due to the presence of only
 288 two Tb^{3+} ions bound to EF-hands 3 and 4 of DREAM($\Delta 64$),
 289 whereas four Tb^{3+} ions are bound to CaM.¹⁰ Nonetheless, it is
 290 also possible that the presence of Tyr100 at position 7 of the
 291 EF-hand 3 binding loop and Tyr139 at position 10 of EF-hand
 292 4 on CaM provides a more efficient energy transfer to Tb^{3+} .³⁸

293 Detailed analysis of DREAM($\Delta 64$) excitation spectra due to
 294 the $^5\text{D}_4 \rightarrow ^7\text{F}_5$ transition at 545 nm shows a broad peak with
 295 maxima at 280 and 32 nm fwhm (Figure 3a). The ratio of
 296 terbium luminescence intensity upon excitation at 295 and 280
 297 nm is 0.40, which indicates that tyrosine and tryptophan
 298 residues are able to transfer energy.³⁹ The excitation spectra of
 299 DREAM($\Delta 160$), DREAM(E186Q), and DREAM(E234Q) are
 300 identical to those of DREAM($\Delta 64$), with a broader fwhm of 36
 301 nm and a higher 295 nm/280 nm ratio of 0.52 for
 302 DREAM($\Delta 161$). Analysis of the C-terminal domain of
 303 DREAM shows the presence of three tyrosine residues
 304 (Y174, Y195, and Y203); however, only Y174 is within the
 305 range of 5–10 Å necessary for an efficient energy transfer to
 306 Tb^{3+} bound at EF-hands 3 and 4 (Figure 3b).^{40,41} Therefore, to
 307 quantify the energy transfer contribution of Y174, we
 308 constructed a DREAM(Y174A) mutant and determined the
 309 effect of this mutation on the sensitized emission and excitation
 310 spectra. This mutant shows an identical circular dichroism

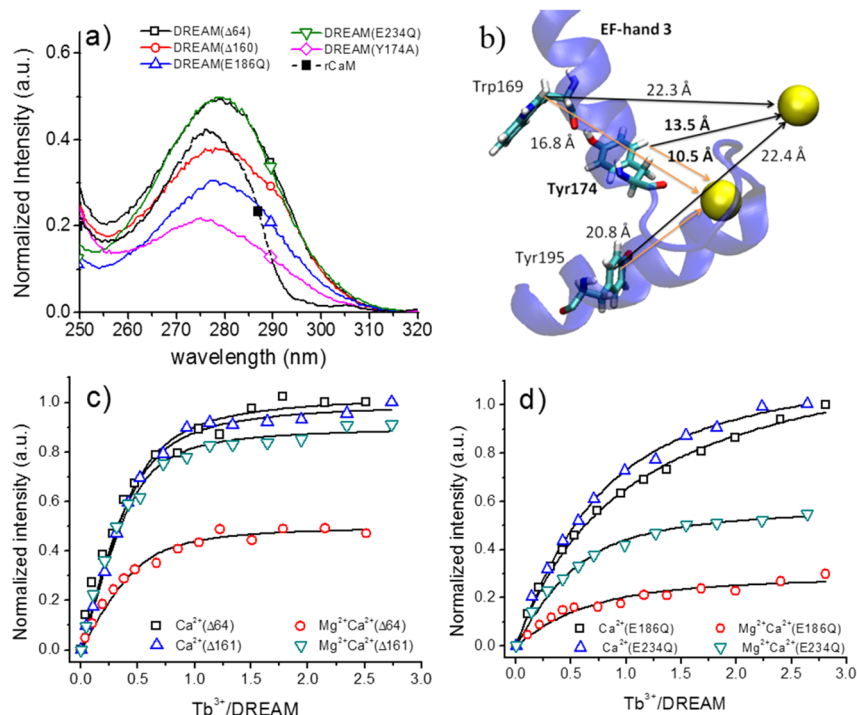


Figure 3. (a) Excitation spectra of DREAM constructs bound to Tb³⁺ (20 μM protein with 40 μM Tb³⁺). The spectra were normalized so that the intensity corresponding to backbone to Tb³⁺ energy transfer at 240 nm is the same for DREAM(Δ64), DREAM(Δ160), and DREAM(Y174A) while the magnitude is half for DREAM(E186Q) and DREAM(E234Q). (b) Calcium/terbium binding sites of EF-hands 3 and 4. Only EF-hand 3 is shown (blue) for the sake of clarity. (c) Titrations of Tb³⁺ into DREAM(Δ64) and DREAM(Δ160) in 20 mM TRIS (pH 7.4) and 100 μM Ca²⁺ with and without 5 mM Mg²⁺. (d) Titration of Tb³⁺ into DREAM(E186Q) and DREAM(E234Q) under the conditions described for panel c. Solid lines represent the best fit using the quadratic equation for *N* binding sites.

311 transition and amplitude as well as the same Tb³⁺-induced
 312 tryptophan fluorescence change, as the DREAM(Δ64)
 313 construct (data not shown). On the other hand, the efficiency
 314 of energy transfer in the DREAM(Y174A) mutant is decreased
 315 by ~60%, judging from the decreased sensitized emission at
 316 545 nm (Figure 3a). The excitation spectra of this construct
 317 also show a 5 nm blue shift to 275 nm with a fwhm of 38 nm
 318 and a 295 nm/280 nm ratio of 0.41. The decrease in the
 319 sensitized emission and the blue shift of the excitation spectra
 320 support the role of Y174 as an energy donor, while the identical
 321 295 nm/280 nm ratio for DREAM(Δ64) and DREAM-
 322 (Y174A) is indicative of Tyr → Trp → Tb³⁺ being the
 323 predominant energy transfer pathway. The similar Tb³⁺
 324 sensitization observed in DREAM(Δ161) and DREAM(Δ64)
 325 constructs indicates that aromatic amino acids at the N-
 326 terminus do not transfer energy to Tb³⁺ and that the observed
 327 luminescence arises from terbium bound at EF-hands 3 and 4.
 328 For comparison, the excitation spectra of CaM are also shown,
 329 and a characteristic maximum at 277 nm with fwhm of 24 nm
 330 and a 295 nm/280 nm ratio of 0.07 is observed, which is in
 331 good agreement with a Tyr → Tb³⁺ energy transfer. Moreover,
 332 the lack of vibronic structures on the excitation spectra on all
 333 constructs indicates that phenylalanine residues do not play a
 334 major role in energy transfer.

335 The shorter distance from Tyr174 to EF-hand 3 (10.5 Å)
 336 than to EF-hand 4 (13.5 Å) supports the idea that monitoring
 337 the binding of Tb³⁺ using the sensitized emission may allow us
 338 to identify whether aromatic amino acids on DREAM can
 339 transfer energy to Tb³⁺ bound at both EF-hands. To confirm
 340 this hypothesis, we employed two DREAM constructs in which
 341 glutamic acid at position 12 of the calcium binding loop has

342 been mutated to glutamine, thus inactivating either EF-hand 3
 343 in DREAM(E186Q) or EF-hand 4 in DREAM(E234Q).⁴² As
 344 expected, the excitation spectra of Tb³⁺ bound at EF-hand 3 in
 345 the DREAM(E234Q) mutant show fluorescence ~39% greater
 346 than that of Tb³⁺ bound at EF-hand 4 in the DREAM(E186Q)
 347 mutant (Figure 3a).

348 Titration of Tb³⁺ into Ca²⁺-bound DREAM(Δ64) or
 349 DREAM(Δ161) shows that both construct have a similar
 350 affinity for Tb³⁺ in the presence of calcium. The dissociation
 351 constant obtained using the quadratic equation shows identical
 352 affinity for Tb³⁺ in the presence of Ca²⁺ with a *K_d* of 1.8 ± 0.6
 353 μM for DREAM(Δ64) and a *K_d* of 1.6 ± 0.2 μM for
 354 DREAM(Δ161). Interestingly, in the presence of 5 mM MgCl₂,
 355 the sensitized emission of Tb³⁺ is decreased by 53% for
 356 DREAM(Δ64) but no significant changes are observed for
 357 DREAM(Δ161) (Figure 3c). To better understand the
 358 mechanism of binding of Tb³⁺ to EF-hands 3 and 4 of
 359 DREAM, we have also conducted titrations in the presence of
 360 Ca²⁺ or Mg²⁺ and Ca²⁺ using the DREAM(E186Q) and
 361 DREAM(E234Q) protein mutants (Figure 3d). Displacement
 362 of Ca²⁺ from DREAM(E186Q) by Tb³⁺ shows a weaker
 363 dissociation constant of 11 ± 1 μM compared to that of
 364 DREAM(E234Q) (5.9 ± 0.5 μM). However, a decrease in the
 365 sensitized emission upon addition of 5 mM MgCl₂ similar to
 366 that for DREAM(Δ64) was observed, with emission decreases
 367 of 55 and 80% for DREAM(E234Q) and DREAM(E186Q),
 368 respectively (Figure 3d). Under the conditions used for these
 369 titrations (500 μM CaCl₂ or 500 μM CaCl₂ and 5 mM MgCl₂),
 370 Tb³⁺ binds first to the inactivated EF-hand (see ITC
 371 experiments below). Therefore, the data shown in Figure 3d
 372 highlight the fact that binding of Mg²⁺ to EF-hand 2 induces

Table 1. Fluorescence and Anisotropy Decay Parameters of DREAM($\Delta 64$) Bound to Ca^{2+} or Tb^{3+} ^a

| | $\bar{\tau}_1$ (f_1) (ns) | w_1 (ns) | τ_2 (f_2) (ns) | $\langle \tau \rangle$ (ns) | Θ_1 (f_1) (ns) | Θ_2 (f_2) (ns) | χ^2 |
|---------------------------------------|-------------------------------|------------|-------------------------|-----------------------------|---------------------------|---------------------------|----------|
| apoDREAM($\Delta 64$) | 1.8 (0.39) | 0.69 | 5.7 (0.61) | 4.2 | 0.40 (0.35) | 15 (0.65) | 0.5 |
| Ca^{2+} DREAM($\Delta 64$) | 1.5 (0.48) | 0.60 | 5.9 (0.52) | 3.8 | 0.52 (0.40) | 29 (0.60) | 0.9 |
| Tb^{3+} DREAM($\Delta 64$) | 1.5 (0.47) | 0.64 | 5.8 (0.53) | 3.8 | 0.23 (0.58) | 27 (0.42) | 1.5 |

^aValues in parentheses represent the fraction intensity and fractional depolarization. τ_1 is the mean decay time of the Gaussian distribution with a width of distribution w_1 . The lifetime of the discrete single-exponential term is denoted as τ_2 . The average lifetime, $\langle \tau \rangle$, was calculated using eqs 1 and 2 of the Supporting Information. α_1 and α_2 are normalized pre-exponential decay fractions and f_1 and f_2 exponential decay fractions.

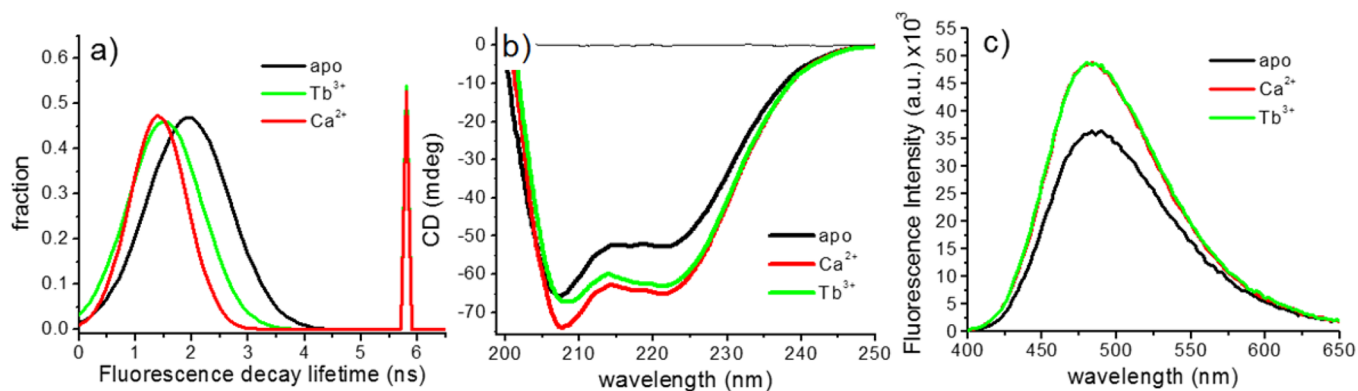


Figure 4. (a) Tryptophan fluorescence lifetime distribution of DREAM($\Delta 64$) in the presence of Ca^{2+} or Tb^{3+} . Decay data were modeled as a Gaussian distribution and a discrete decay (parameters listed in Table 1). (b) Circular dichroism spectra of $40 \mu\text{M}$ DREAM($\Delta 64$) in the presence of 1 mM Ca^{2+} , 2 mM EDTA, or $160 \mu\text{M}$ Tb^{3+} in 5 mM TRIS (pH 7.4). (c) Binding of Tb^{3+} or Ca^{2+} to $10 \mu\text{M}$ DREAM($\Delta 64$) in the presence of $40 \mu\text{M}$ 1,8-ANS.

373 structural rearrangements that have a greater impact on EF-
374 hand 3. This is in good agreement with the fact that EF-hand 2
375 is adjacent to EF-hand 3, and that the exiting helix of EF-hand 2
376 is in direct contact with the entering helix of EF-hand 3 (Figure
377 1a). Tryptophan 169 and tyrosine 174, both of which are
378 shown to play a major role in energy transfer, both reside on
379 the entering helix of EF-hand 3. The presence of Mg^{2+} also
380 enhanced the binding of Tb^{3+} , with dissociation constants of
381 $5.8 \pm 1.9 \mu\text{M}$ for DREAM(E186Q) and $2.7 \pm 0.4 \mu\text{M}$ for
382 DREAM(E234Q). This increase in apparent affinity is likely
383 due to a decrease in the level of nonspecific binding of Tb^{3+} to
384 secondary sites or to EF-hand 2. Together, these results support
385 a model in which terbium displaces Ca^{2+} from EF-hand 4 and
386 EF-hand 3 and highlight the role of Mg^{2+} binding at EF-hand 2
387 as a structural cofactor in DREAM.

388 **Binding of Terbium(III) to DREAM Leads to a**
389 **Structural Rearrangement Similar to Those Observed**
390 **for Ca^{2+} .** The terbium(III)-induced tryptophan emission
391 quenching observed in Figure 2b supports the idea that Tb^{3+}
392 is able to mimic the structural changes induced by binding of
393 Ca^{2+} to EF-hands 3 and 4. To test whether binding of Tb^{3+} to
394 DREAM induces a structural transition analogue to that of
395 Ca^{2+} , we monitored the fluorescence and anisotropy decay of
396 Trp169, the fluorescence of the extrinsic hydrophobic probe
397 1,8-ANS bound at the C-terminus of DREAM($\Delta 64$),¹³ and
398 changes in secondary structure. Detailed information regarding
399 the environment and dynamics of Trp169 and how they are
400 affected by metal binding can be obtained by measuring the
401 fluorescence and anisotropy decay lifetimes. As previously
402 reported,⁴³ the fluorescence decay of Trp169 on DREAM-
403 ($\Delta 64$) was best fitted by a Gaussian-discrete bimodal decay
404 model, whose parameters are listed in Table 1 and shown in
405 Figure 4a. The small discrepancies between our results and
406 those published previously likely arise from the lack of LDAO
407 detergent under our conditions. Nonetheless, we observe that

408 addition of Ca^{2+} or Tb^{3+} results in a decrease in the average
409 excited-state lifetime from 4.8 to 3.8 ns, which is due to a
410 decrease in the fractional intensity contribution of the long
411 lifetime and a slightly faster Gaussian decay from 1.8 to 1.5 ns.
412 The lack of significant lifetime quenching of Trp169 by Tb^{3+} is
413 likely due to the poor efficiency of this energy transfer process.
414 Moreover, anisotropy decay measurements were conducted to
415 identify whether binding of Tb^{3+} induces dimerization of
416 DREAM as observed for Ca^{2+} . The frequency domain
417 anisotropy decay data were best fitted with a double discrete
418 model, in which the fast Θ_1 is associated with fast local
419 fluctuations of tryptophan and the slow Θ_2 corresponds to the
420 global rotation of the protein (Table 1). A clear transition from
421 15 to 29 ns upon binding of Ca^{2+} and 27 ns in the presence of
422 Tb^{3+} is observed. These rotational correlation times match well
423 with the values of 14 ns for a monomeric and 28 ns for a
424 dimeric DREAM($\Delta 64$) protein approximated by the Einstein–
425 Stokes equation at $17 \text{ }^\circ\text{C}$, $\eta = 0.0100 \text{ P}$, and 0.73 g/mL
426 hydration. Differences in rotational correlation times of the fast
427 local tryptophan motion can be observed between Ca^{2+} - and
428 Tb^{3+} -bound DREAM($\Delta 64$), where a 2-fold faster local motion
429 is measured in the presence of terbium (0.52 ns vs 0.23 ns). In
430 the metal-free DREAM($\Delta 64$), the local flexibility accounts for
431 35% of the depolarization, while in the Ca^{2+} - and Tb^{3+} -bound
432 DREAM($\Delta 64$) form, this rotation contributes 48 and 58% to
433 depolarization, respectively. Altogether, excited-state and
434 anisotropy decay of Trp169 reveals that even though binding
435 of Tb^{3+} can induce dimerization of DREAM($\Delta 64$) this metal
436 also induces a more dynamic structure near the Trp169
437 compared to Ca^{2+} .

As shown in Figure 4b, the CD spectrum of metal-free
438 DREAM($\Delta 64$) shows a characteristic profile with minima at
439 222 and 208 nm (the maximum at 190 nm is not shown) in
440 good agreement with an α -helical structure. Upon binding of
441 Ca^{2+} , an ellipticity decrease at 200–225 nm and an increase at 442

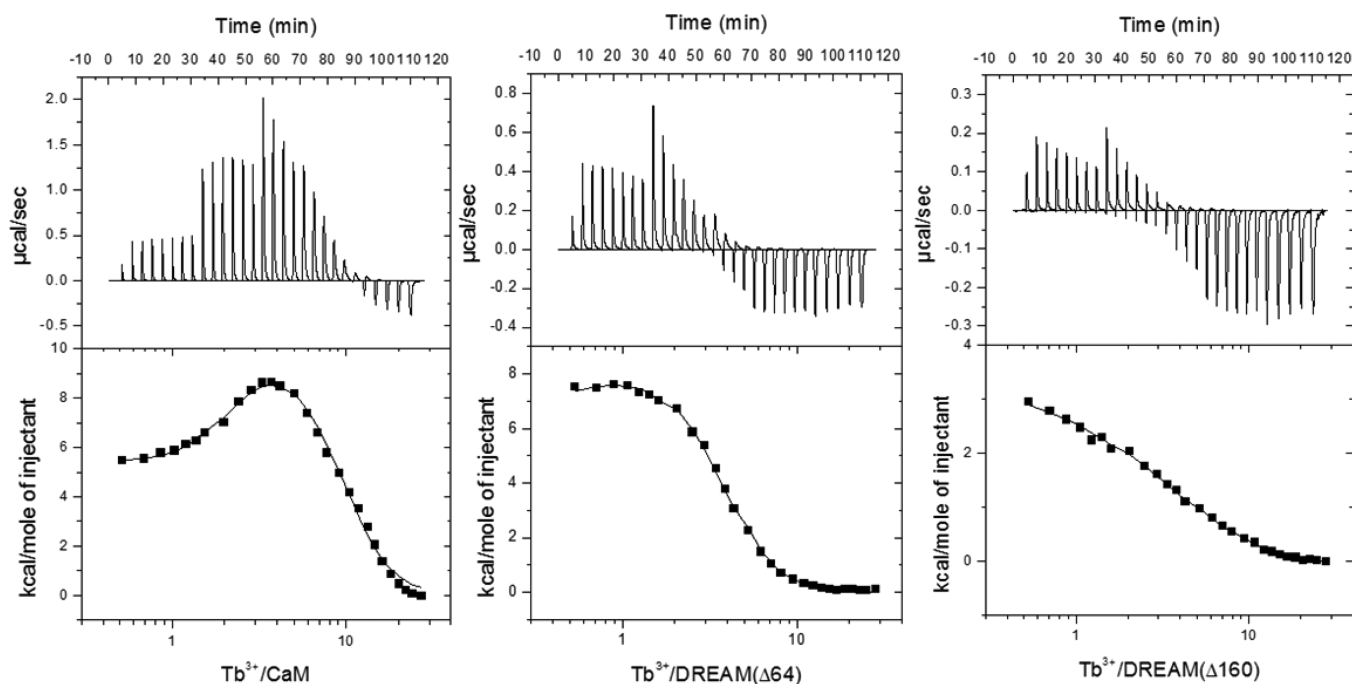


Figure 5. ITC isotherms for Tb^{3+} displacement of Ca^{2+} from CaM, DREAM($\Delta 64$), and DREAM($\Delta 160$). The top panels of each profile reflect the thermal power expressed in units of microcalories per second. The bottom panels show integrated reaction heats (ΔH) expressed in units of kilocalories per mole. The solid lines present the best fitting curve with the parameters listed in Table 2.

443 190 nm are observed, which can be explained by an increase in
 444 α -helical content and/or rearrangement of the α -helices. On
 445 the other hand, in the presence of Tb^{3+} , a CD spectrum
 446 intermediate between those measured for apo and Ca^{2+} -bound
 447 DREAM is observed. This intermediate structure was also
 448 observed when a 2-fold excess of terbium was added to a
 449 sample containing 100 μM calcium (not shown). The largest
 450 deviation in CD spectra between Ca^{2+} - and Tb^{3+} -bound
 451 DREAM($\Delta 64$) is observed near the 208 nm minimum. Thus,
 452 the CD data indicate that Tb^{3+} is able to displace Ca^{2+} and
 453 induce a structural change distinct from those observed for
 454 metal-free and Ca^{2+} -bound DREAM($\Delta 64$).

455 Despite the small differences in the protein dynamics near
 456 Trp169, as well as the deviation in secondary structure upon
 457 binding of Tb^{3+} , we observed similar binding of 1,8-ANS at the
 458 C-terminal hydrophobic cavity of DREAM($\Delta 64$).¹³ The
 459 fluorescence emission of this probe has been extensively
 460 shown to be sensitive to the immediate environment, and while
 461 the total intensity upon Ca^{2+} binding is observed to increase, no
 462 changes in fluorescence of 1,8-ANS were observed upon
 463 displacement of Ca^{2+} by Tb^{3+} (Figure 4c). Moreover, frequency
 464 domain analysis of the excited state of 1,8-ANS as well as the
 465 depolarization time reveals no significant differences between
 466 Ca^{2+} - and Tb^{3+} -bound DREAM($\Delta 64$) (data not shown).
 467 Overall, the indication is that the hydrophobic cavity exposure
 468 induced by calcium is also triggered by terbium.

469 **DREAM Binds Tb^{3+} through an Entropy-Driven**
 470 **Mechanism.** To complement the Tb^{3+} :DREAM binding
 471 studies using sensitized emission, we also conducted calorimetric
 472 studies in which the heat associated with Tb^{3+}
 473 displacement of Ca^{2+} bound at the EF-hands of CaM and
 474 DREAM is measured. Isothermal calorimetry reveals that
 475 displacement of Ca^{2+} from CaM is endothermic and can be best
 476 modeled as a sequential process (Figure 5a). The profile of the
 477 ITC isotherm for Tb^{3+} displacement of Ca^{2+} bound to CaM is

similar to that obtained for binding of calcium to a plant– 478
 mammalian CaM chimera,⁴⁴ albeit with slightly different 479
 thermodynamic parameters. The associations of Tb^{3+} ions 480
 with CaM at EF-hands 1–4 have association constants slightly 481
 lower than those determined for Ca^{2+} binding, which is likely 482
 due to competition effects. We associate the site with K_1 483
 parameters as representing the displacement of Ca^{2+} by Tb^{3+} , 484
 while the two other observed binding processes (K_2 and K_3) 485
 likely arise from a convolution of specific and nonspecific 486
 association of Tb^{3+} ions. The presence of nonspecific binding 487
 of Tb^{3+} ions is supported by the fact that addition of 5 mM Mg^{2+} 488
 results in drastic changes in the thermodynamic parameters 489
 associated with K_2 and K_3 . The observed decreases in enthalpy 490
 and entropy of ~ 160 and ~ 280 kcal mol⁻¹ for K_2 and K_3 , 491
 respectively, also support the idea that these supplementary 492
 sites are strikingly different and may involve different ligands 493
 and/or ion displacement. We associate the thermodynamic 494
 values recovered in the presence of Mg^{2+} with the displacement 495
 of Ca^{2+} specifically bound at the loops of EF-hands 1–4, 496
 convoluted with any additional protein rearrangement to 497
 accommodate Tb^{3+} . It can be observed that in the presence 498
 of Mg^{2+} there is a 3-fold decrease in affinity for the K_1 site, with 499
 a minimal change in enthalpy and entropy, whereas sites K_2 and 500
 K_3 show similar affinity, with K_2 having an enthalpy and 501
 entropy 2-fold larger than those of K_3 sites. Altogether, these 502
 values can be interpreted as corresponding to Tb^{3+} displace- 503
 ment of Ca^{2+} ions from four EF-hands with K_1 representing the 504
 weakest Ca^{2+} binding hand and K_2 and K_3 corresponding to the 505
 three remaining EF-hands. Following previous studies in which 506
 calmodulin was shown to follow a sequential filling of EF-hands 507
 1 \rightarrow 2 \rightarrow 3 and 4 by Tb^{3+} and Ca^{2+} , we associate the K_1 binding 508
 site to that of binding of Tb^{3+} to EF-hand 4.^{32,45} Interestingly, 509
 EF-hand 4 in calmodulin shows the presence of glutamic acid at 510
 position 11 near the $-z$ metal coordination (Figure 1), which 511
 may explain the smaller enthalpic and entropic contribution 512

Table 2. ITC Parameters Recovered for Tb³⁺ Displacement of Ca²⁺ from EF-Hands of CaM and DREAM Using a Sequential Model^a

| | $K_1 \times 10^4$ | $K_2 \times 10^4$ | $K_3 \times 10^4$ | ΔH_1 | ΔH_2 | ΔH_3 | $T\Delta S_1$ | $T\Delta S_2$ | $T\Delta S_3$ |
|-------------------------------------|-------------------|-------------------|-------------------|--------------|--------------|--------------|---------------|---------------|---------------|
| CaM | 29 ± 4.2 | 0.7 ± 0.4 | 5.1 ± 8.4 | 12 ± 5 | 212 ± 38 | -307 ± 127 | 19 ± 3.9 | 217 | -302 |
| CaM with Mg ²⁺ | 8.9 ± 1.8 | 1.9 ± 0.2 | 1.4 ± 0.2 | 13 ± 1.5 | 47 ± 0.6 | 23 ± 7 | 20 ± 1.4 | 52 ± 0.6 | 28 ± 7 |
| DREAM(Δ64) | 22 ± 1.3 | 8.1 ± 1.6 | 2.8 ± 0.2 | 13 ± 9.0 | 18 ± 0.6 | -2.5 ± 2.7 | 20 ± 9.1 | 24 ± 0.4 | 3.6 ± 2.7 |
| DREAM(Δ64) with Mg ²⁺ | 16 ± 2.5 | 11 ± 1.1 | 6.0 ± 0.5 | 12 ± 1.3 | 18 ± 6.0 | 3.4 ± 3.2 | 19 ± 1.3 | 25 ± 5.9 | 9.9 ± 3.1 |
| DREAM (Δ160) | 6.9 ± 3.2 | 8.9 ± 9.2 | | 13 ± 1.7 | 8.2 ± 1.3 | | 19 ± 1.5 | 15 ± 1.1 | |
| DREAM (Δ160) with Mg ²⁺ | 6.8 ± 1.4 | 1.8 ± 0.6 | | 11 ± 2.2 | 7.7 ± 2.4 | | 17 ± 2.1 | 14 ± 2.4 | |
| DREAM (E186Q) with Mg ²⁺ | 14.0 ± 0.9 | 8.6 ± 1.3 | 8.8 ± 2.2 | 7.5 ± 1.2 | 15 ± 1.7 | 2.2 ± 2.6 | 14 ± 0.8 | 22 ± 1.8 | 9 ± 2.7 |
| DREAM (E234Q) with Mg ²⁺ | 5.7 ± 0.9 | 27 ± 1.5 | 16 ± 6.2 | 11 ± 1.9 | 3.6 ± 2.7 | 4.0 ± 1.3 | 18 ± 1.9 | 9.6 ± 2.5 | 11 ± 0.9 |

^aAll experiments were conducted in triplicate at 25 °C; errors are standard deviations. Enthalpy and entropy changes shown in units of kilocalories per mole; association constants in units of inverse molar.

513 upon displacement of Ca²⁺ by Tb³⁺. The Tb³⁺ binding sites
514 corresponding to K_2 show ΔH_2 and ΔS_2 thermodynamic
515 parameters that are ~2-fold larger than those of ΔH_3 and ΔS_3 ,
516 which is likely due to two Tb³⁺ binding sites being reported by
517 the K_2 parameters. This allows us to approximate a ΔH value of
518 ~23 kcal mol⁻¹ and a $T\Delta S$ of ~27 kcal mol⁻¹ for Tb³⁺
519 displacement of Ca²⁺ bound at EF-hands 1–3 and a ΔH of
520 13 kcal mol⁻¹ and a $T\Delta S$ of 28 kcal mol⁻¹ for EF-hand 4.

521 Furthermore, displacement of Ca²⁺ bound to DREAM(Δ64)
522 by Tb³⁺ shows a simpler isotherm (Figure Sb), which is similar
523 to that obtained for displacement of Ca²⁺ by Tm³⁺ in the
524 *Entamoeba histolytica* calcium binding protein.¹⁴ Despite the
525 ability to model the isotherm using the simpler one-set-of-sites
526 model, we decided to present the results obtained from a three-
527 site sequential model based on three accounts. First, it is
528 expected that binding of Tb³⁺ is not associated with a
529 cooperative behavior because the protein undergoes a transition
530 from a calcium-bound structure to a calcium-like structure.
531 Second, replacement of glutamic acid at position 12 of the loop
532 in EF-hand 3 resulted in an isotherm that could not be fitted by
533 a one-set-of-sites model. Lastly, displacement of Ca²⁺ by Tb³⁺
534 in other calcium binding proteins with known calcium
535 cooperativity have been observed to follow a sequential
536 mechanism.^{14,44} The recovered parameters using the sequential
537 model are listed in Table 2. For the sake of completeness, the
538 parameters recovered with an N -set-of-sites model are
539 presented in Table S1. The data reveal that three Tb³⁺ ions
540 can bind to DREAM(Δ64), with slightly different affinities,
541 such that $K_1 > K_2 > K_3$. Interestingly, the associated enthalpy
542 and entropy of sites K_1 and K_2 are similar to those found for
543 Ca²⁺ displacement of K_1 sites on CaM, while the enthalpy and
544 entropy of the site corresponding to K_3 show significantly lower
545 enthalpic and entropic contributions. Titration of Tb³⁺ in the
546 presence of Ca²⁺ and 5 mM Mg²⁺ in DREAM(Δ64) increases
547 $\Delta\Delta H_3$ and $T\Delta\Delta S_3$ by ~6 kcal mol⁻¹, while the enthalpy and
548 entropy of sites K_1 and K_2 remain unchanged. Unlike CaM, in
549 which all four EF-hands are believed to prefer binding to Ca²⁺
550 versus Mg²⁺, EF-hand 2 on DREAM is proposed to bind Mg²⁺
551 preferentially.^{8,10} Therefore, we assign the recovered thermody-
552 namic parameters for sites with K_1 and K_2 association constants
553 as representing Ca²⁺ displacement from EF-hand 3 or 4 while
554 those recovered for the site with K_3 being representative of
555 binding of Tb³⁺ to EF-hand 2. The assignment of K_3 to EF-
556 hand 2 is also supported by the displacement of Ca²⁺ by Tb³⁺ in
557 a DREAM(Δ160) construct lacking the Mg²⁺ binding EF-hand
558 2, which shows only two sites with affinities and thermody-
559 namic parameters similar to those of K_1 and K_2 on
560 DREAM(Δ64). The recovered association constant and

thermodynamic parameter for binding of Tb³⁺ to DREAM-
561 (Δ160) are also independent of Mg²⁺, in agreement with the
562 sensitized emission titrations. However, despite the similarities,
563 a decrease of ~10 kcal mol⁻¹ in the enthalpy and entropy for
564 the K_2 site is observed for DREAM(Δ160) compared to that of
565 DREAM(Δ64). This decrease in energetics could be due to a
566 distinct metal coordination or loss of structural rearrangement
567 at the missing N-terminus. It is tempting to assign the K_2
568 parameters of DREAM(Δ160) as representing binding of Tb³⁺
569 to EF-hand 3, due to closer proximity to the now deleted N-
570 terminal domain, but these results do not permit unequivocal
571 assignment. Together, the recovered thermodynamic paramete-
572 rs for DREAM(Δ64) and DREAM(Δ160) show that Tb³⁺
573 can efficiently displace Ca²⁺ from the C-terminal EF-hands 3
574 and 4, and that deletion of the N-terminal amino acids (1–160)
575 results in modification of the metal binding properties of EF-
576 hands 3 and 4. Thus, we can approximate a ΔH value of ~15
577 kcal mol⁻¹ and a $T\Delta S$ of ~22 kcal mol⁻¹ for Tb³⁺ displacement
578 of Ca²⁺ bound at EF-hands 3 and 4 of DREAM(Δ64).
579

Additional experiments in which we monitored the
580 thermodynamics of association of Tb³⁺ with Ca²⁺-bound
581 DREAM(E186Q) with inactivated EF-hand 3 and DREAM-
582 (E234Q) with inactivated EF-hand 4 were also conducted, and
583 the recovered parameters are listed in Table 2. Displacement of
584 Ca²⁺ by Tb³⁺ on the DREAM(E186Q) construct is best
585 modeled as a three-site sequential binding process, in which the
586 K_1 site has the highest affinity, while ΔH_1 and ΔS_1 are ~5 kcal
587 mol⁻¹ lower than those obtained for DREAM(Δ64). Tb³⁺
588 binding at the site with K_2 shows an affinity identical to that
589 observed for K_2 on DREAM(Δ64) in the presence of Mg²⁺, and
590 similar enthalpic and entropic contributions. The third site, K_3 ,
591 shows parameters similar to those recovered for Tb³⁺ binding at
592 EF-hand 2 of DREAM(Δ64) and likely corresponds to the
593 same binding process. The decrease in enthalpy and entropy
594 upon binding of Tb³⁺ at the site with K_1 as well as its stronger
595 binding affinity compared to those of K_2 and K_3 seems to
596 indicate that this site likely corresponds to the inactivated EF-
597 hand 3. The fact that only small changes are observed upon
598 mutation of glutamic acid at position 12 (–z coordination) to
599 glutamine supports the idea that this site may still be weakly
600 bound to either Ca²⁺ or Mg²⁺. Interestingly, these results also
601 show that the E186Q substitution does not affect the binding of
602 Tb³⁺ at EF-hand 3, which is interesting but not unexpected.
603 This effect is likely due to weaker binding of Ca²⁺, which in turn
604 facilitates Tb³⁺ association.
605

The DREAM(E234Q) construct, in which EF-hand 4 is
606 inactivated, is also able to bind three Tb³⁺ ions with ranges of
607 affinities similar to those obtained for the DREAM(Δ64) in the
608

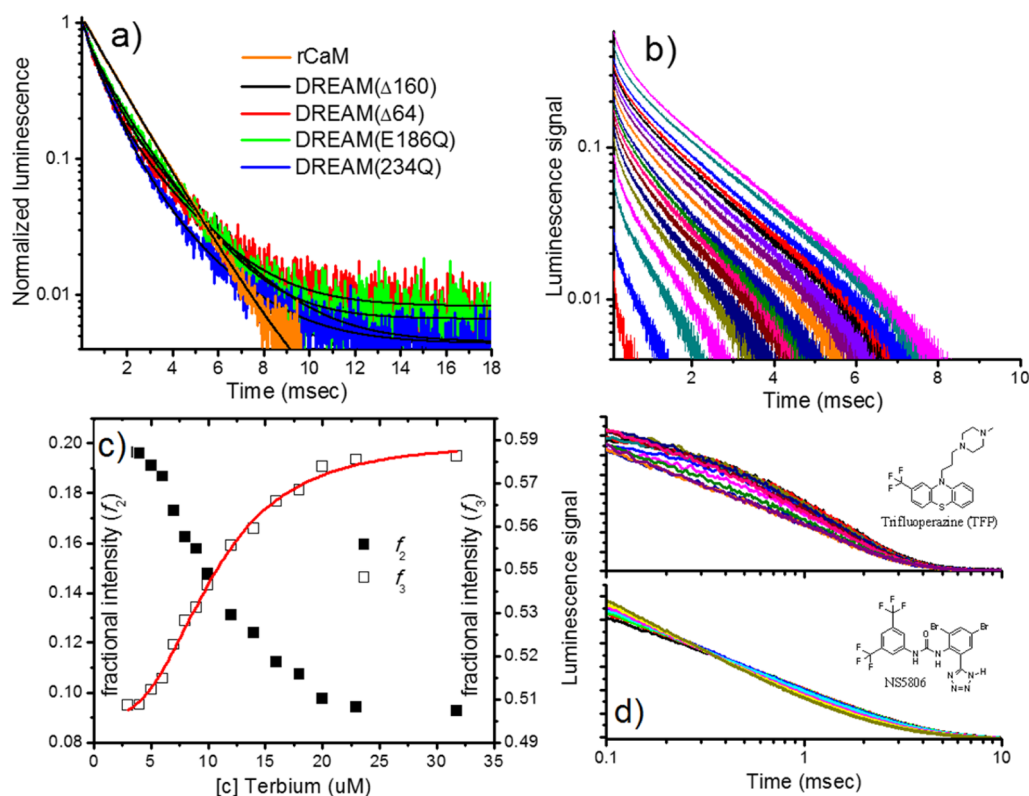


Figure 6. (a) Luminescence decay of Tb^{3+} bound to CaM and constructs of DREAM, with 4:1 Tb^{3+} :CaM and 2:1 Tb^{3+} :DREAM stoichiometric ratios. Solid lines represent the best fit using Globals software analysis, and recovered parameters listed in Table 3. (b) Luminescence intensity decay profiles as a function of Tb^{3+} binding to 10 μM DREAM($\Delta 64$). The luminescence decays in panel b were analyzed using a triple discrete model, and the fractional intensity contribution of the two slowest lifetimes is shown in c. The fastest decay component had a lifetime of $\sim 80 \mu\text{s}$ with a $< 10\%$ contribution and is not shown. (d) Luminescence decay of Tb^{3+} bound to DREAM and DREAM($\Delta 64$) as a function of the hydrophobic molecules TFP (top) bound to DREAM and NS5806 (bottom) bound to DREAM.

609 presence of Mg^{2+} . In this construct, the site with association
 610 constant K_2 binds stronger, followed by K_3 and then K_1 sites.
 611 However, the enthalpy for site K_2 on DREAM(E234Q) is 5-
 612 fold lower than those obtained for K_2 on DREAM($\Delta 64$). The
 613 sites with a K_3 association constant show an enthalpy and an
 614 entropy identical to those of the site corresponding to K_3 on
 615 DREAM($\Delta 64$). In fact, the enthalpy and entropy for sites K_2
 616 and K_3 are much closer to those obtained for binding of Tb^{3+} to
 617 EF-hand 2 of DREAM($\Delta 64$) in the presence of Mg^{2+} , with a
 618 ΔH of $\sim 4 \text{ kcal mol}^{-1}$ and a ΔS of $\sim 10 \text{ kcal mol}^{-1}$. These
 619 results suggest that inactivation of EF-hand 4 likely results in a
 620 weak binding of Ca^{2+} or Mg^{2+} , both of which can be easily
 621 displaced by Tb^{3+} (based on higher K_2 and K_3) with a
 622 concomitant lower enthalpic and entropic contribution.
 623 Overall, ITC demonstrates that in the presence of saturating
 624 amounts of calcium, the Glu \rightarrow Gln mutation at position 12 of
 625 the EF-hand metal binding loop actually facilitates binding of
 626 Tb^{3+} .

627 **Luminescence Decay of Tb^{3+} -Bound DREAM Is**
 628 **Sensitive to Ligand Binding.** Sensitized emission studies
 629 show that Mg^{2+} is able to induce changes in the emission of
 630 bound Tb^{3+} ; to further study this effect, we decided to
 631 determine if Mg^{2+} can induce structural changes within the
 632 coordination sphere of Tb^{3+} . We employed direct excitation of
 633 Tb^{3+} using the 355 nm line of a Nd:YAG pulsed laser and
 634 measured the luminescence decay of terbium bound to the EF-
 635 hands of CaM and DREAM constructs. This approach permits
 636 analysis of the local environment at the binding site of Tb^{3+}
 637 ions, namely the EF-hand loops. Additionally, this method has

been widely used to monitor changes in the coordination 638
 sphere of lanthanides as well as the effects of water 639
 coordination.⁴⁶ Following the studies described above, we 640
 first characterized the luminescence decay of Tb^{3+} bound to 641
 CaM, and as expected, the luminescence decay shown in Figure 642 16
 6a follows a monoexponential decay with a τ_1 of 1.38 ms. A 643 16
 single-exponential decay of approximately 1 ms has been 644
 reported for the Tb^{3+} :CaM complex, and double-exponential 645
 decays have been observed for complexes of Eu^{3+} and 646
 calmodulin.^{30,33} 647

Luminescence decay of Tb^{3+} bound to DREAM($\Delta 64$) shows 648
 a τ_1 lifetime of 0.86 ms (59%) and a τ_2 lifetime of 2.20 ms 649
 (14%), whereas Tb^{3+} bound to DREAM($\Delta 160$) decays with a 650
 τ_1 lifetime of 0.74 ms (54%) and a τ_2 lifetime of 2.16 ms (29%). 651
 The faster lifetime likely corresponds to a contribution from 652
 partially coordinated Tb^{3+} ions and is similar to the 780 μs 653
 decay obtained for Tb^{3+} bound to NTA in water.³⁴ We and 654
 others have determined the lifetime of Tb^{3+} in buffer at pH 7.4 655
 to be $450 \pm 30 \mu\text{s}$; therefore, we associate τ_1 to represent Tb^{3+} 656
 bound to a weak coordination site on DREAM.⁴⁷ The second 657
 lifetime is much longer than that determined for Tb^{3+} bound to 658
 parvalbumin (1.3 ms) or CaM (1.38 ms) but is similar to that 659
 of Eu^{3+} bound to these proteins or complexes of Tb^{3+} and 660
 bimetallic ligand in which no water coordination is 661
 observed.^{30,34,48} Long-lived excited-state decays are observed 662
 for lanthanides with little phonon quenching that often is due 663
 to limited water access.⁴⁷ Interestingly, addition of 100 mM 664
 NaCl reduces the fast lifetime to values similar to those of Tb^{3+} 665
 in water and increases the fractional intensity of the long 666 13

lifetime component ~ 3 -fold (Table 3). The luminescence decay of Tb^{3+} was not significantly affected by LDAO, a

Table 3. Terbium(III) Luminescence Decay Parameters Recovered upon Binding to DREAM and DREAM Constructs^a

| | τ_1 (ms) | f_1 | τ_2 (ms) | f_2 |
|--|---------------|-------|---------------|-------|
| CaM | 1.38 | 1.00 | | |
| CaM with TFP ^b | 0.46 | 0.31 | 1.36 | 0.69 |
| DREAM($\Delta 64$) | 0.86 | 0.59 | 2.22 | 0.14 |
| DREAM($\Delta 64$) with Mg^{2+} | 0.74 | 0.54 | 2.05 | 0.24 |
| DREAM($\Delta 64$)(a) ^c | 0.58 | 0.27 | 2.00 | 0.69 |
| DREAM($\Delta 64$)(b) ^c | 0.46 | 0.17 | 2.04 | 0.77 |
| DREAM($\Delta 64$)(c) ^c with NSS806 | 0.43 | 0.58 | 1.83 | 0.39 |
| DREAM($\Delta 160$) | 0.75 | 0.47 | 2.16 | 0.29 |
| DREAM($\Delta 160$) with Mg^{2+} | 0.63 | 0.41 | 2.03 | 0.37 |
| DREAM(E186Q) | 0.62 | 0.50 | 2.02 | 0.27 |
| DREAM(E186Q) with Mg^{2+} | 0.48 | 0.47 | 1.58 | 0.42 |
| DREAM(E234Q) | 0.63 | 0.27 | 1.75 | 0.46 |
| DREAM(E234Q) with Mg^{2+} | 0.45 | 0.31 | 1.70 | 0.48 |

^aAll shown parameters were recovered using a triple or double discrete exponential decay; the error of the reported values is 2.5% on average. All experiments were conducted at room temperature ($\sim 20^\circ\text{C}$) at protein concentration of $20\ \mu\text{M}$ with addition of $80\ \mu\text{M}\ \text{Tb}^{3+}$ for CaM and $40\ \mu\text{M}\ \text{Tb}^{3+}$ for DREAM constructs. An additional lifetime of $\sim 80\ \mu\text{s}$ was resolved for all DREAM constructs, likely due to parasitic light or PMT recovery delay, and is not shown. ^bMeasured in the presence of $131\ \mu\text{M}$ TFP. ^cThe protein concentration for these experiments was $10\ \mu\text{M}$ in the presence of (a) $100\ \text{mM}$ NaCl, (b) $100\ \text{mM}$ NaCl and $10\ \text{mM}$ LDAO, or (c) $100\ \text{mM}$ NaCl, $10\ \text{mM}$ LDAO, and $31\ \mu\text{M}$ NSS806.

detergent that has been proposed to stabilize DREAM in a single conformation.¹² Titration of Tb^{3+} into DREAM($\Delta 64$) in the presence of $100\ \text{mM}$ NaCl and $10\ \text{mM}$ LDAO shows that the fractional intensity of the τ_2 lifetime increases in a dose-dependent manner and saturates at a stoichiometric ratio of 2:1, whereas the fractional intensity of τ_1 decreases (Figure 6b,c). Additional measurements of the luminescence decay of the DREAM construct with inactivated EF-hands show similar bimodal exponential decays. One of the most salient observations is that the decay lifetime of DREAM(E234Q) is significantly shorter [$\tau_2 = 1.75\ \text{ms}$ (27%)] than that observed for DREAM(E186Q) [$\tau_2 = 2.02\ \text{ms}$ (46%)]. This indicates that binding of Tb^{3+} at EF-hand 4 induces a restructuring of the coordination sphere similar to that induced when both EF-hands 3 and 4 are bound to Tb^{3+} . On the other hand, the structural arrangement of the binding loop at EF-hand 3 when Tb^{3+} is bound at this site is significantly different, with a much more solvent-exposed Tb^{3+} ion. However, it could also be possible that these two lifetimes cannot be separately resolved in the DREAM($\Delta 64$) decays. The lifetime of Tb^{3+} bound at the solvent-exposed site is identical on both constructs, with τ_1 being $0.62\ \text{ms}$ (50%) for DREAM(E186Q) and τ_1 being $0.63\ \text{ms}$ (27%) for DREAM(E234Q), but faster than that observed for the fully active proteins. Interestingly, in the presence of $5\ \text{mM}\ \text{Mg}^{2+}$, a decrease in the decay lifetimes and an increase in the intensity contribution of the long-lived decay are observed for all constructs, except for DREAM(E234Q). The observed changes are largest for DREAM(E186Q) where a decrease of $0.44\ \text{ms}$ in τ_2 is also accompanied by a 15% increase in the contribution of this decay component. The decay lifetimes, $\tau_1 = 0.74\ \text{ms}$ for DREAM($\Delta 64$) and $\tau_1 = 0.63\ \text{ms}$ for DREAM-

($\Delta 160$), are still longer than those for Tb^{3+} in water, while those of DREAM(E186Q) and DREAM(E234Q) are identical to that of Tb^{3+} in water. The effect of Mg^{2+} on the luminescence data is in good agreement with the changes observed in the sensitized emission titrations (Figure 3d).

Finally, we examined whether Tb^{3+} luminescence decay would be sensitive to structural changes induced on CaM and DREAM upon binding of small hydrophobic ligands. To test this hypothesis, we chose trifluoperazine (TFP) and a novel biphenyl-urea compound named NSS806. These compounds have been shown to bind at hydrophobic cavities on CaM and DREAM, respectively, in a calcium-dependent manner.^{20,49} Upon titration of each ligand into Tb^{3+} -bound CaM and DREAM($\Delta 64$), we observe a strong dose-dependent modulation of the luminescence decay (Figure 6d). Global analysis of the luminescence decay of the Tb^{3+} -CaM and Tb^{3+} -DREAM($\Delta 64$) complexes reveals that binding of these small hydrophobic ligands induces a decrease in intensity contribution from τ_2 on both constructs while also decreasing the long lifetime on DREAM($\Delta 64$). Plotting the change in f_2 as a function of TFP or NSS806 concentration yields dissociation constants of $\sim 37\ \mu\text{M}$ for both ligands (data not shown), which is larger than those observed in the Ca^{2+} -bound form of these proteins ($K_d \sim 1\ \mu\text{M}$ for TFP, and $K_d = 5\ \mu\text{M}$ for NSS806). The discrepancies could be due to secondary sites being populated (TFP has been shown to bind at four sites on CaM with dissociation constants between $1\ \mu\text{M}$ and $5\ \text{mM}$) or to the distinct conformation of the hydrophobic cavity of the proteins in the Tb^{3+} -bound form.

Displacement of Ca^{2+} by Tb^{3+} Induces Minimal Changes in the Collisional Cross Section of DREAM. To further study the displacement of Ca^{2+} ions from the EF-hand domains of DREAM, as well as to determine the magnitude of the structural differences between the Ca^{2+} - and Tb^{3+} -bound DREAM structures, ion mobility measurements were conducted to determine the ion-neutral collisional cross section using a TIMS-MS analyzer (see Table 4). The mass spectrum

Table 4. Experimental and Theoretical Ion-Neutral Collision Cross Sections for the DREAM($\Delta 64$): Ca^{2+} / Tb^{3+} Molecular Ions

| | +7 (\AA^2) | +8 (\AA^2) | +9 (\AA^2) |
|---|-----------------------|-----------------------|-----------------------|
| theoretical ^a | | | |
| DREAM($\Delta 64$): Ca^{2+} Ca^{2+} | 2773 | 2798 | 2825 |
| experimental | | | |
| DREAM($\Delta 64$): Ca^{2+} Ca^{2+} | 2225 | 2243 | 2297 |
| DREAM($\Delta 64$): Ca^{2+} Tb^{3+} | 2205 | 2231 | 2260 |
| DREAM($\Delta 64$): Tb^{3+} Tb^{3+} | 2200 | 2228 | 2238 |

^aCalculated using the IMoS software as described in Materials and Methods.

of DREAM($\Delta 64$) under native nanoESI conditions shows a narrow charge-state distribution (+7 to +9), with multiple Ca^{2+} and Tb^{3+} adducts. A closer look at the charge distribution shows the presence of the apo form, $[\text{M} + n\text{H}]^{n+}$, as well as three adduct series: $[\text{M} + \text{Ca}^{2+}_{x=1-3} + (n-x)\text{H}]^{n+}$, $[\text{M} + \text{Ca}^{2+}_x + \text{Tb}^{3+}_y + (n-x-y)\text{H}]^{n+}$, and $[\text{M} + \text{Tb}^{3+}_{x=1-2} + (n-x)\text{H}]^{n+}$ [see the example of the +8 charge-state distribution of DREAM($\Delta 64$) in the presence of Ca^{2+} , Ca^{2+} and Tb^{3+} , and Tb^{3+} in Figure 7a]. Inspection of the mobility profiles for each adduct series shows that as the charge state increases from +7 to +9, a decrease in mobility (and increase in CCS) is observed as a consequence of the interaction of the molecular ion with the

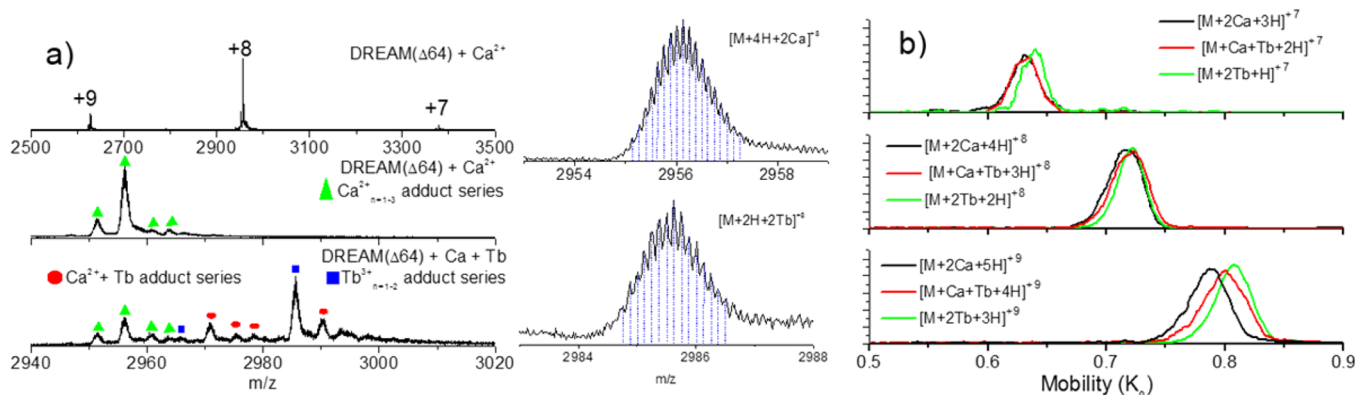


Figure 7. (a) Typical nanoESI mass spectra of DREAM($\Delta 64$) in the presence of Ca^{2+} and DREAM($\Delta 64$) in the presence of Ca^{2+} and Tb^{3+} . The isotopic distributions of the DREAM($\Delta 64$): 2Ca^{2+} and DREAM($\Delta 64$): 2Tb^{3+} complexes are shown for the sake of clarity. (b) NanoESI TIMS mobility spectra of DREAM($\Delta 64$) bound to Ca^{2+} and/or Tb^{3+} .

external electric field, which is not necessarily an indication of conformational changes. However, small changes in the CCS are observed as a function of the adduct series within each charge state. For example, a decrease in the CCS is observed for DREAM($\Delta 64$) bound to Tb^{3+} when compared to that of DREAM($\Delta 64$) bound to Ca^{2+} and DREAM($\Delta 64$) bound to Ca^{2+} and Tb^{3+} (see Figure 7b). Comparison of the observed CCS profiles ($\text{CCS}_{+7 \rightarrow +9} = 2200\text{--}2300 \text{ \AA}^2$) to that of a previously reported 2JUL NMR structure of DREAM⁷ ($\text{CCS}_{\text{theo}} = 2773 \text{ \AA}^2$) suggests that the gas-phase conformations are more compact than that observed in solution, probably as a consequence of the interaction of the adduct with the EF-hand domains in the absence of the solvent. In addition, the higher affinity of Tb^{3+} when compared to that of Ca^{2+} may induce a more compact structure (smaller CCS) for DREAM($\Delta 64$) bound to Tb^{3+} than for DREAM($\Delta 64$) bound to Ca^{2+} and DREAM($\Delta 64$) bound to Ca^{2+} and Tb^{3+} in the absence of the solvent.

DISCUSSION

In this report, we present conclusive evidence that Tb^{3+} is able to bind at the C-terminus of DREAM and displace Ca^{2+} from the binding loop at EF-hands 3 and 4. Using circular dichroism as well as fluorescence intensity and anisotropy decay of intrinsic fluorescent probes, we demonstrate that Tb^{3+} is able to induce structural changes on DREAM identical to those observed upon Ca^{2+} binding. Circular dichroism shows a small deviation of the spectra near 208 nm, a region that is sensitive to the presence of antiparallel β -sheets.⁵⁰ DREAM is mainly α -helical, and the only region in which small antiparallel β -sheets are formed is between the metal binding loops of each EF-hand pair.⁷ Therefore, it is possible that association of Tb^{3+} induces structural changes at the metal binding loop that result in a loss of these short β -sheet regions. Small differences between Tb^{3+} - and Ca^{2+} -bound DREAM were also observed by anisotropy decay measurements. Anisotropy decay revealed that dimers are formed in the Ca^{2+} - or Tb^{3+} -bound form of DREAM, but binding of Tb^{3+} induces a more dynamic environment near Trp169. Using molecular dynamics, we have previously shown that Trp169 in DREAM($\Delta 64$) can populate two rotamers, and it is possible that Tb^{3+} binding could enhance this rotamer transition, which would result in an increase in local dynamics.⁴³

As seen for other calcium binding proteins, we observe that aromatic amino acids at the C-terminus are able to transfer

energy to the bound Tb^{3+} . Specifically, we show that mutation of Y174 to alanine results in a significant reduction ($\sim 60\%$) in the sensitized emission of Tb^{3+} at 545 nm, while maintaining identical 280 nm/295 nm ratios compared to that of DREAM($\Delta 64$). Together, these results highlight the presence of an antenna effect, in which W169 is the main donor to Tb^{3+} . Attempts to use sensitized emission and Tb^{3+} titrations to elucidate the lanthanide binding sequence to EF-hands 3 and 4 on DREAM indicate that both EF-hands bind Tb^{3+} with a similar affinity [$K_d = 5.9 \mu\text{M}$ for DREAM(E234Q), and $K_d = 11 \mu\text{M}$ for DREAM(E186Q)]. Because these experiments were conducted in the presence of excess calcium and magnesium, inactivation of each EF-hand actually favors binding to the mutated loop (see ITC results). Therefore, we are unable to identify whether the slightly lower affinity of Tb^{3+} with the DREAM(E186Q) mutant is due to the inherent lower affinity to this hand or because a metal ion (Ca^{2+} or Mg^{2+}) is loosely bound at this mutated site. Nonetheless, one of the most salient observations of these Tb^{3+} titration experiments is that in the presence of Mg^{2+} , the sensitized emission of Tb^{3+} decreases by more than 50%. This decrease in intensity at 545 nm could be due to either Mg^{2+} -induced structural rearrangements of the environment near Trp169 or rearrangement of the Tb^{3+} binding loop at EF-hands 3 and 4. Indeed, we observe that EF-hand 3, which is next to EF-hand 2, is more sensitive to magnesium binding. These results support the idea that Mg^{2+} plays a structural role in DREAM and that at physiological concentrations it may act as a functional cofactor through interaction with EF-hand 2.

Isothermal calorimetry experiments show that Tb^{3+} displacement of Ca^{2+} from EF-hands 3 and 4 on DREAM($\Delta 64$) in the presence of 5 mM Mg^{2+} is associated with a ΔG of $-14 \text{ kcal mol}^{-1}$, while the displacement energy for the DREAM($\Delta 160$) construct is $-12 \text{ kcal mol}^{-1}$. The same displacement process for EF-hands 1–4 in CaM is associated with a free energy ΔG of $-18 \text{ kcal mol}^{-1}$. The more favorable displacement of Ca^{2+} from CaM EF-hands compared to DREAM($\Delta 64$) highlights the stronger association of Ca^{2+} in the latter.⁴² Throughout this report, we correlate the K_1 thermodynamic parameters with displacement of Ca^{2+} from EF-hand 3 and K_2 with displacement from EF-hand 4 in the DREAM($\Delta 64$), DREAM(E186Q), and DREAM(E234Q) constructs. Even though these correlations are not unequivocally proven by our results, they are supported by the associated changes in enthalpy and entropy under different conditions. Following this assignment, we can

837 approximate the enthalpy and entropy associated with
 838 coordination of Tb^{3+} by Glu at position 12 of EF-hands 3
 839 and 4 by calculating $\Delta H_{Glu}^{(Mutant)} = \Delta H_i^{DREAM(\Delta 64)} -$
 840 $\Delta H_i^{DREAM(Mutant)}$ and $T\Delta S_{Glu}^{(Mutant)} = T\Delta S_i^{DREAM(\Delta 64)} -$
 841 $T\Delta S_i^{DREAM(Mutant)}$, where the subscript i is 1 for DREAM-
 842 (E186Q) and 2 for DREAM(E234Q). These calculations reveal
 843 that coordination of Tb^{3+} by Glu186 of EF-hand 3 is associated
 844 with a $\Delta H_{Glu}^{(E186Q)}$ of 4.5 kcal mol⁻¹ and a $T\Delta S_{Glu}^{(E186Q)}$ of 5.0
 845 kcal mol⁻¹. In contrast, Glu234 of EF-hand 4 has a 3-fold larger
 846 enthalpy and entropy contribution, with a $\Delta H_{Glu}^{(E234Q)}$ of 14
 847 kcal mol⁻¹ and a $T\Delta S_{Glu}^{(E234Q)}$ of 15 kcal mol⁻¹. In both cases,
 848 coordination of the metal ion is driven by favorable entropy
 849 contributions, likely due to release of a water molecule upon
 850 coordination of Glu at position 12. These results are similar to
 851 those observed for Ca^{2+} binding to CaM and DREAM($\Delta 64$) in
 852 which entropy was observed to be the main driving force.^{42,44}
 853 In contrast, the enthalpic contribution due to metal binding to
 854 the EF-hands of CaM and DREAM($\Delta 64$) has been shown to
 855 be very small. It is possible that the unfavorable endothermic
 856 process observed here is due to additional structural changes
 857 associated with Glu12 coordination. The larger enthalpy and
 858 entropy associated with coordination of Glu12 on EF-hand 4
 859 highlights the role of this EF-hand in controlling the activation
 860 of DREAM. Indeed, Glu12 is positioned on the exiting helix of
 861 EF-hand 4 that is immediately adjacent to a hydrophobic cavity
 862 that mediates the calcium-regulated co-assembly with potas-
 863 sium channels and small ligands.^{20,51,52}
 864 Another interesting aspect of the recovered thermodynamic
 865 parameters shown in Table 2 is that the enthalpy and entropy
 866 recovered for all the titrations are highly correlated. This
 867 correlation has been observed before for Ca^{2+} binding to
 868 CaM⁴⁴ as well as in other systems.⁵³ More importantly, the
 869 linear relationship of $T\Delta S$ as a function of ΔH allows us to
 870 extrapolate the entropy associated with displacement of Ca^{2+} ,
 871 prior to any structural change induced by Tb^{3+} (Figure 8). This

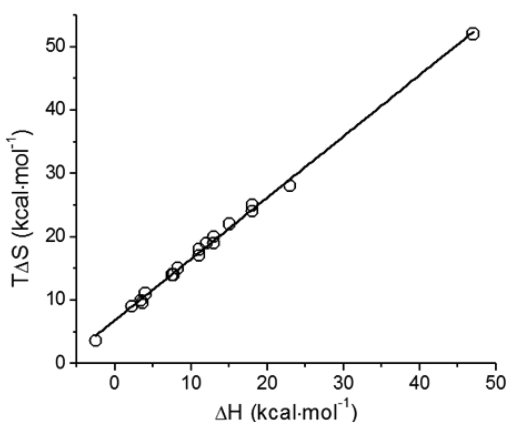


Figure 8. Plot of $T\Delta S$ vs ΔH for Tb^{3+} displacement of Ca^{2+} from DREAM($\Delta 64$), DREAM($\Delta 161$), DREAM(E186Q), DREAM(E234Q), and CaM. The solid line represents the best linear fit to the data.

872 is based on the idea that displacement of Ca^{2+} by Tb^{3+} is not
 873 associated with the formation or breakage of any new bond
 874 because the coordinations of Ca^{2+} and Tb^{3+} in bulk water are
 875 identical. Extrapolating the linear relationship yields a
 876 $T\Delta S_{displacement}$ value of 6.9 ± 0.2 kcal mol⁻¹, which is similar
 877 to the value obtained for binding of Ca^{2+} to metal-free CaM in
 878 which $T\Delta S_{bind} = 7.2 \pm 0.1$ kcal mol⁻¹.⁴⁴ A possible explanation

for the entropic gain could be due to an increase in the 879
 dynamics of the protein, something that is supported by the 880
 anisotropy decay data. The correlation of enthalpy and entropy 881
 can also be explained by a process that involves the release of 882
 water following the association of two ions of opposite charges 883
 in solution. The resulting charge neutralization would facilitate 884
 the mobilization of solvent molecules from the surface of the 885
 protein into the bulk water.⁵⁴ This release of water molecules is 886
 associated with an unfavorable endothermic process (breakage 887
 of water–protein hydrogen bonds) and favorable positive 888
 change in entropy. Indeed, Ca^{2+} -bound DREAM($\Delta 64$) (net 889
 charge of -3 at pH 7.4) and Ca^{2+} -bound CaM (net charge of 890
 -16 at pH 7.4) would be neutralized by 2 and 8 units upon 891
 Tb^{3+} displacement, respectively. This charge neutralization 892
 effect could also partially account for the decreased enthalpy 893
 and entropy contribution of the DREAM(E186Q) and 894
 DREAM(E234Q) mutants, both of which have one less 895
 negative charge than DREAM($\Delta 64$) does. 896

Sensitized emission, circular dichroism, TIMS–MS, and ITC 897
 experiments provide information about global structural 898
 changes of the protein upon displacement of Ca^{2+} by Tb^{3+} . 899
 On the other hand, luminescence studies allow us to gain better 900
 insight into the immediate coordination sphere of Tb^{3+} ion, and 901
 how this environment is affected by inactivation of EF-hands, 902
 Mg^{2+} binding, ionic strength, and/or ligand binding. Measure- 903
 ments of the luminescence decay of Tb^{3+} bound to different 904
 constructs highlight the idea that Tb^{3+} bound at EF-hand 3 is 905
 more solvent-exposed than Tb^{3+} bound at EF-hand 4. 906
 Nonetheless, the decay observed for DREAM($\Delta 64$) is much 907
 slower than that observed for CaM, indicating that the 908
 coordination around Tb^{3+} in DREAM greatly restricts the 909
 accessibility of water. We also observe that the luminescence 910
 decays are widely affected by addition of excess Mg^{2+} , 911
 supporting the idea that some secondary sites of Tb^{3+} binding, 912
 including EF-hand 2 on DREAM, are identical to those of Mg^{2+} 913
 binding. The high sensitivity of EF-hand 3 to Mg^{2+} binding 914
 could also be due to propagated rearrangement of EF-hand 2 915
 upon association of Mg^{2+} . It is also possible that binding of 916
 Mg^{2+} at these secondary sites is responsible for the observed 917
 rearrangement of the EF-hand loops. The overall picture that 918
 emerges from these observations is that Mg^{2+} is able to 919
 modulate the protein structure and that secondary metal sites 920
 may play a role in modulating protein conformation. Indeed, 921
 previous work and our unpublished results support the idea 922
 that two Ca^{2+} specific sites and additional secondary sites are 923
 found on DREAM($\Delta 160$).¹⁰ Lastly, titration of small hydro- 924
 phobic ligands also reveals that the environment near the metal 925
 binding loops of EF-hands 3 and 4 is sensitive to association of 926
 ligand with DREAM. Altogether, these observations highlight 927
 the idea that association of these small molecules at the 928
 hydrophobic surfaces of CaM and DREAM induces conforma- 929
 tional changes that not only can distort the coordination 930
 geometry of Tb^{3+} at the binding loops but also could 931
 potentially facilitate dissociation of Tb^{3+} from the protein. 932

Finally, ion mobility and mass spectrometry measurements 933
 support the hypothesis that Tb^{3+} can displace Ca^{2+} from EF- 934
 hands 3 and 4 and that the resulting folded conformation of the 935
 Tb^{3+} -bound DREAM($\Delta 64$) protein is almost identical to that 936
 of the calcium-bound protein during native ESI conditions. 937
 Comparison of the observed CCS profiles to that of a 938
 previously reported NMR structure of DREAM⁷ suggested 939
 that the gas-phase conformations are more compact than that 940
 observed in solution, probably as a consequence of the 941

942 interaction of the adduct with the EF-hand domains in the
943 absence of the solvent. In addition, the higher affinity of Tb^{3+}
944 when compared to that of Ca resulted in more compact
945 structures (smaller CCS) for DREAM($\Delta 64$) bound to Tb^{3+}
946 than for DREAM($\Delta 64$) bound to Ca^{2+} and DREAM($\Delta 64$)
947 bound to Ca^{2+} and Tb^{3+} in the absence of the solvent.

948 ■ CONCLUSION

949 In this report, we show compelling evidence supporting the
950 specific association of Tb^{3+} with EF-hands 3 and 4 of DREAM.
951 We also demonstrate that replacement of Ca^{2+} with Tb^{3+} leads
952 to an increase in the dynamics of the protein; however, the
953 structural and functional properties between DREAM bound to
954 either metal are highly similar. We show that like the case for
955 CaM, Tb^{3+} bound to DREAM can be sensitized by aromatic
956 amino acids at the C-terminus, with tryptophan 169 being the
957 main energy donor. The high affinity of the EF-hands for Tb^{3+}
958 and the fluorescence properties of this lanthanide have allowed
959 us to highlight the role of Mg^{2+} as a structural cofactor, which
960 can bind to EF-hand 2 and modify the immediate environment
961 near the calcium binding loops of EF-hands 3 and 4. Isothermal
962 calorimetry also highlights the role of EF-hand 4 in mediating
963 calcium-regulated ligand recognition in DREAM. These
964 findings provide structural information about DREAM and
965 will facilitate future structural NMR studies and lanthanide
966 resonance energy transfer experiments aimed at exploring the
967 association of DREAM with other proteins.

968 ■ ASSOCIATED CONTENT

969 ● Supporting Information

970 The Supporting Information is available free of charge on the
971 ACS Publications website at DOI: [10.1021/acs.biochem.6b00067](https://doi.org/10.1021/acs.biochem.6b00067).

972 Recovered parameters from fitting of the ITC isotherms
973 using an N -set-of-sites model (PDF)

975 ■ AUTHOR INFORMATION

976 Corresponding Author

977 *Department of Chemistry and Biochemistry, Florida International
978 University, 11200 SW 8th St., Miami, FL 33199. Phone:
979 305-3487406. Fax: 305-3483772. E-mail: miksovsk@fiu.edu.

980 Funding

981 This work was supported by the National Science Foundation
982 (MCB 1021831, J.M.) and the National Institutes of Health
983 (Grant R00GM106414, F.F.-L.). W.G.G. was fully supported by
984 National Institute of General Medical Sciences Grant R25
985 GM061347.

986 Notes

987 The authors declare no competing financial interest.

988 ■ ABBREVIATIONS

989 DREAM, downstream regulatory element antagonist modu-
990 lator; CaM, calmodulin; fwhm, full width at half-maximum;
991 KChIP, potassium channel-interacting protein; DREAM($\Delta 64$),
992 mouse DREAM construct lacking residues 1–64; 1,8-ANS, 8-
993 anilinonaphthalene-1-sulfonic acid; CD, circular dichroism;
994 TIMS-MS, trapped ion mobility spectrometry–mass spec-
995 trometry; TFP, trifluoperazine.

■ REFERENCES

- 996
997 (1) Carrion, A. M., Link, W. A., Ledo, F., Mellstrom, B., and Naranjo, 997
998 J. R. (1999) DREAM is a Ca^{2+} -regulated transcriptional repressor. 998
999 *Nature* 398, 80–84. 999
1000 (2) Buxbaum, J. D., Choi, E., Luo, Y., Lilliehook, C., Crowley, A. C., 1000
1001 Merriam, D. E., and Wasco, W. (1998) Calsenilin: A calcium-binding 1001
1002 protein that interacts with the presenilins and regulates the levels of a 1002
1003 presenilin fragment. *Nat. Med.* 4, 1177–1181. 1003
1004 (3) An, W. F., Bowlby, M. R., Betty, M., Cao, J., Ling, H., Mendoza, 1004
1005 G., Hinson, J. W., Mattsson, K. I., Strassle, B. W., Trimmer, J. S., and 1005
1006 Rhodes, K. J. (2000) Modulation of A-type potassium channels by a 1006
1007 family of calcium sensors. *Nature* 403, 553–556. 1007
1008 (4) Cheng, H. M., Pitcher, G. M., Laviolette, S. R., Whishaw, I. Q., 1008
1009 Tong, K. I., Kockeritz, L. K., Wada, T., Joza, N. A., Crackower, M., 1009
1010 Goncalves, J., Sarosi, I., Woodgett, J. R., Oliveira-dos-Santos, A. J., 1010
1011 Ikura, M., van der Kooy, D., Salter, M. W., and Penninger, J. M. (2002) 1011
1012 DREAM is a critical transcriptional repressor for pain modulation. *Cell* 1012
1013 108, 31–43. 1013
1014 (5) Costigan, M., and Woolf, C. J. (2002) No DREAM, no pain: 1014
1015 Closing the spinal gate. *Cell* 108, 297–300. 1015
1016 (6) Fontán-Lozano, Á., Romero-Granados, R., del-Pozo-Martín, Y., 1016
1017 Suárez-Pereira, I., Delgado-García, J. M., Penninger, J. M., and Carrión, 1017
1018 Á. M. (2009) Lack of DREAM protein enhances learning and memory 1018
1019 and slows brain aging. *Curr. Biol.* 19, 54–60. 1019
1020 (7) Lusin, J. D., Vanarotti, M., Li, C., Valiveti, A., and Ames, J. B. 1020
1021 (2008) NMR structure of DREAM: Implications for Ca^{2+} -dependent 1021
1022 DNA binding and protein dimerization. *Biochemistry* 47, 2252–2264. 1022
1023 (8) da Silva, A. C., Kendrick-Jones, J., and Reinach, F. C. (1995) 1023
1024 Determinants of ion specificity on EF-hands sites. conversion of the 1024
1025 Ca^{2+}/Mg^{2+} site of smooth muscle myosin regulatory light chain into a 1025
1026 Ca^{2+} -specific site. *J. Biol. Chem.* 270, 6773–6778. 1026
1027 (9) Gifford, J., Walsh, M., and Vogel, H. (2007) Structures and 1027
1028 metal-ion-binding properties of the Ca^{2+} -binding helix-loop-helix EF- 1028
1029 hand motifs. *Biochem. J.* 405, 199–221. 1029
1030 (10) Craig, T. A., Benson, L. M., Venyaminov, S. Y., Klimtchuk, E. S., 1030
1031 Bajzer, Z., Prendergast, F. G., Naylor, S., and Kumar, R. (2002) The 1031
1032 metal-binding properties of DREAM. *J. Biol. Chem.* 277, 10955– 1032
1033 10966. 1033
1034 (11) Kretsinger, R. H., and Nockolds, C. E. (1973) Carp muscle 1034
1035 calcium-binding protein. II. structure determination and general 1035
1036 description. *J. Biol. Chem.* 248, 3313–3326. 1036
1037 (12) Osawa, M., Tong, K. I., Lilliehook, C., Wasco, W., Buxbaum, J. 1037
1038 D., Cheng, H.-Y. M., Penninger, J. M., Ikura, M., and Ames, J. B. 1038
1039 (2001) Calcium-regulated DNA binding and oligomerization of the 1039
1040 neuronal calcium-sensing protein, Calsenilin/DREAM/KChIP3. *J.* 1040
1041 *Biol. Chem.* 276, 41005–41013. 1041
1042 (13) Gonzalez, W. G., and Miksovská, J. (2014) Application of ANS 1042
1043 fluorescent probes to identify hydrophobic sites on the surface of 1043
1044 DREAM. *Biochim. Biophys. Acta, Proteins Proteomics* 1844, 1472–1480. 1044
1045 (14) Mustafi, S. M., Mukherjee, S., Chary, K. V. R., Del Bianco, C., 1045
1046 and Luchinat, C. (2004) Energetics and mechanism of Ca^{2+} 1046
1047 displacement by lanthanides in a calcium binding protein. *Biochemistry* 1047
1048 43, 9320–9331. 1048
1049 (15) Martin, B., and Richardson, F. S. (1979) Lanthanides as probes 1049
1050 for calcium in biological systems. *Q. Rev. Biophys.* 12, 181–209. 1050
1051 (16) Rao, S. T., Satyshur, K. A., Greaser, M. L., and Sundaralingam, 1051
1052 M. (1996) X-ray structures of mn, cd and tb metal complexes of 1052
1053 troponin C. *Acta Crystallogr., Sect. D: Biol. Crystallogr.* 52, 916–922. 1053
1054 (17) Pintacuda, G., Park, A. Y., Keniry, M. A., Dixon, N. E., and 1054
1055 Otting, G. (2006) Lanthanide labeling offers fast NMR approach to 1055
1056 3D structure determinations of Protein-Protein complexes. *J. Am.* 1056
1057 *Chem. Soc.* 128, 3696–3702. 1057
1058 (18) Gonzalez, W., and Miksovská, J. (2015) Characterization of the 1058
1059 photophysical, thermodynamic and structural properties of the 1059
1060 terbium (III)-KChIP3 complex. *Biophys. J.* 108, 218a. 1060
1061 (19) Gonzalez, W. G., Arango, A. S., and Miksovská, J. (2015) 1061
1062 Amphiphilic residues 29–44 of DREAM N-termini mediate calm- 1062
1063 odulin:DREAM complex formation. *Biochemistry* 54, 4391–4403. 1063

- 1064 (20) Gonzalez, W. G., Pham, K., and Miksovská, J. (2014)
1065 Modulation of the voltage-gated potassium channel (Kv4.3) and the
1066 auxiliary protein (KChIP3) interactions by the current activator
1067 NS5806. *J. Biol. Chem.* 289, 32201–32213.
- 1068 (21) George, S. E., Su, Z., Fan, D., and Means, A. R. (1993)
1069 Calmodulin-cardiac troponin C chimeras. effects of domain exchange
1070 on calcium binding and enzyme activation. *J. Biol. Chem.* 268, 25213–
1071 25220.
- 1072 (22) Fernandez-Lima, F., Kaplan, D., and Park, M. (2011) Note:
1073 Integration of trapped ion mobility spectrometry with mass
1074 spectrometry. *Rev. Sci. Instrum.* 82, 126106.
- 1075 (23) Fernandez-Lima, F., Kaplan, D. A., Suetering, J., and Park, M. A.
1076 (2011) Gas-phase separation using a trapped ion mobility
1077 spectrometer. *Int. J. Ion Mobility Spectrom.* 14, 93–98.
- 1078 (24) Molano-Arevalo, J. C., Hernandez, D. R., Gonzalez, W. G.,
1079 Miksovská, J., Ridgeway, M. E., Park, M. A., and Fernandez-Lima, F.
1080 (2014) Flavin adenine dinucleotide structural motifs: From solution to
1081 gas phase. *Anal. Chem.* 86, 10223–10230.
- 1082 (25) Hernandez, D. R., DeBord, J. D., Ridgeway, M. E., Kaplan, D. A.,
1083 Park, M. A., and Fernandez-Lima, F. (2014) Ion dynamics in a trapped
1084 ion mobility spectrometer. *Analyst* 139, 1913–1921.
- 1085 (26) McDaniel, E. W., and Mason, E. A. (1973) *The Mobility and*
1086 *Diffusion of Ions in Gases*, Wiley, New York.
- 1087 (27) Larriba, C., and Hogan, C. J., Jr (2013) Ion mobilities in
1088 diatomic gases: Measurement versus prediction with non-specular
1089 scattering models. *J. Phys. Chem. A* 117, 3887–3901.
- 1090 (28) Larriba, C., and Hogan, C. J. (2013) Free molecular collision
1091 cross section calculation methods for nanoparticles and complex ions
1092 with energy accommodation. *J. Comput. Phys.* 251, 344–363.
- 1093 (29) Ouyang, H., Larriba-Andaluz, C., Oberreit, D. R., and Hogan, C.
1094 J., Jr (2013) The collision cross sections of iodide salt cluster ions in
1095 air via differential mobility analysis-mass spectrometry. *J. Am. Soc. Mass*
1096 *Spectrom.* 24, 1833–1847.
- 1097 (30) Mulqueen, P., Tingey, J. M., and Horrocks, W. D. (1985)
1098 Characterization of lanthanide(III) ion binding to calmodulin using
1099 luminescence spectroscopy. *Biochemistry* 24, 6639–6645.
- 1100 (31) Chaudhuri, D., Horrocks, W. D., Jr, Amburgey, J. C., and Weber,
1101 D. J. (1997) Characterization of lanthanide ion binding to the EF-hand
1102 protein S100 beta by luminescence spectroscopy. *Biochemistry* 36,
1103 9674–9680.
- 1104 (32) Kilhoffer, M., Gerard, D., and Demaille, J. G. (1980) Terbium
1105 binding to octopus calmodulin provides the complete sequence of ion
1106 binding. *FEBS Lett.* 120, 99–103.
- 1107 (33) Austin, R. H., Stein, D. L., and Wang, J. (1987) Terbium
1108 luminescence-lifetime heterogeneity and protein equilibrium con-
1109 formational dynamics. *Proc. Natl. Acad. Sci. U. S. A.* 84, 1541–1545.
- 1110 (34) Horrocks, W. D., and Sudnick, D. R. (1979) Lanthanide ion
1111 probes of structure in biology. laser-induced luminescence decay
1112 constants provide a direct measure of the number of metal-
1113 coordinated water molecules. *J. Am. Chem. Soc.* 101, 334–340.
- 1114 (35) Hagan, A. K., and Zuchner, T. (2011) Lanthanide-based time-
1115 resolved luminescence immunoassays. *Anal. Bioanal. Chem.* 400,
1116 2847–2864.
- 1117 (36) Fisher, J. R., Sharma, Y., Iuliano, S., Picciotti, R. A., Krylov, D.,
1118 Hurley, J., Roder, J., and Jeromin, A. (2000) Purification of
1119 myristoylated and nonmyristoylated neuronal calcium sensor-1 using
1120 single-step hydrophobic interaction chromatography. *Protein Expres-*
1121 *sion Purif.* 20, 66–72.
- 1122 (37) Drabikowski, W., Brzeska, H., and Venyaminov, SYu. (1982)
1123 Tryptic fragments of calmodulin. Ca²⁺- and Mg²⁺-induced conforma-
1124 tional changes. *J. Biol. Chem.* 257, 11584–11590.
- 1125 (38) Hogue, C. W., MacManus, J. P., Banville, D., and Szabo, A. G.
1126 (1992) Comparison of terbium (III) luminescence enhancement in
1127 mutants of EF hand calcium binding proteins. *J. Biol. Chem.* 267,
1128 13340–13347.
- 1129 (39) Brittain, H. G., Richardson, F. S., and Martin, R. B. (1976)
1130 Terbium(III) emission as a probe of calcium(II) binding sites in
1131 proteins. *J. Am. Chem. Soc.* 98, 8255–8260.
- (40) Kleinerman, M. (1969) Energy migration in lanthanide chelates. 1132
J. Chem. Phys. 51, 2370–2381. 1133
- (41) Wallace, R. W., Tallant, E. A., Dockter, M. E., and Cheung, W. 1134
Y. (1982) Calcium binding domains of calmodulin. sequence of fill as 1135
determined with terbium luminescence. *J. Biol. Chem.* 257, 1845– 1136
1854. 1137
- (42) Osawa, M., Dace, A., Tong, K. I., Valiveti, A., Ikura, M., and 1138
Ames, J. B. (2005) Mg²⁺ and Ca²⁺ differentially regulate DNA 1139
binding and dimerization of DREAM. *J. Biol. Chem.* 280, 18008– 1140
18014. 1141
- (43) Pham, K., Dhulipala, G., Gonzalez, W. G., Gerstman, B. S., 1142
Regmi, C., Chapagain, P. P., and Miksovská, J. (2015) Ca²⁺ and Mg²⁺ 1143
modulate conformational dynamics and stability of downstream 1144
regulatory element antagonist modulator. *Protein Sci.* 24, 741–751. 1145
- (44) Gilli, R., Lafitte, D., Lopez, C., Kilhoffer, M., Makarov, A., 1146
Briand, C., and Haiech, J. (1998) Thermodynamic analysis of calcium 1147
and magnesium binding to calmodulin. *Biochemistry* 37, 5450–5456. 1148
- (45) Wang, C. L., Aquaron, R. R., Leavis, P. C., and Gergely, J. 1149
(1982) Metal-binding properties of calmodulin. *Eur. J. Biochem.* 124, 1150
7–12. 1151
- (46) Hungerford, G., Hussain, F., Patzke, G. R., and Green, M. 1152
(2010) The photophysics of europium and terbium polyoxometalates 1153
and their interaction with serum albumin: A time-resolved 1154
luminescence study. *Phys. Chem. Chem. Phys.* 12, 7266–7275. 1155
- (47) Bünzli, J.-C. G., and Eliseeva, S. V. (2011) Basics of lanthanide 1156
photophysics. *Lanthanide Luminescence*, pp 1–45, Springer, Berlin. 1157
- (48) Deiters, E., Song, B., Chauvin, A., Vandevyver, C., Gummy, F., and 1158
Bünzli, J. (2009) Luminescent bimetallic lanthanide bioprobes for 1159
cellular imaging with excitation in the visible-light range. *Chem. - Eur. J.* 1160
15, 885–900. 1161
- (49) Cook, W. J., Walter, L. J., and Walter, M. R. (1994) Drug 1162
binding by calmodulin: Crystal structure of a calmodulin-trifluoper- 1163
azine complex. *Biochemistry* 33, 15259–15265. 1164
- (50) Kelly, S. M., Jess, T. J., and Price, N. C. (2005) How to study 1165
proteins by circular dichroism. *Biochim. Biophys. Acta, Proteins* 1166
Proteomics 1751, 119–139. 1167
- (51) Wang, H., Yan, Y., Liu, Q., Huang, Y., Shen, Y., Chen, L., Chen, 1168
Y., Yang, Q., Hao, Q., Wang, K., and Chai, J. (2007) Structural basis 1169
for modulation of Kv4 K⁺ channels by auxiliary KChIP subunits. *Nat.* 1170
Neurosci. 10, 32–39. 1171
- (52) Pioletti, M., Findeisen, F., Hura, G. L., and Minor, D. L. (2006) 1172
Three-dimensional structure of the KChIP1-Kv4.3 T1 complex reveals 1173
a cross-shaped octamer. *Nat. Struct. Mol. Biol.* 13, 987–995. 1174
- (53) Kuroki, R., and Yutani, K. (1998) Structural and thermodynamic 1175
responses of mutations at a Ca²⁺ binding site engineered into human 1176
lysozyme. *J. Biol. Chem.* 273, 34310–34315. 1177
- (54) Bowman-James, K., Bianchi, A., and García-España, E. (2012) 1178
Anion Coordination Chemistry, John Wiley & Sons, New York. 1179